Morphological assessment of the earliest paradoxidid trilobites (Cambrian Series 3) from Morocco and Spain

J. JAVIER ÁLVARO*†, JORGE ESTEVE* & SAMUEL ZAMORA‡

*Instituto de Geociencias (CSIC-UCM) and Departamento de Paleontología (UCM),
José Antonio Novais 12, 28040 Madrid, Spain
‡Instituto Geológico y Minero de España, Manuel Lasala 44, 9°B, 50006 Zaragoza, Spain

Abstract – A Cambrian immigration event of paradoxidid trilobites has traditionally marked some regional lower–middle Cambrian boundaries in the Acado-Baltic subprovince (including Baltica and the Mediterranean and Avalonian margins of West Gondwana). The earliest paradoxidine species in Morocco and the Iberian Peninsula have been used as a chronostratigraphic link to support the definition of a common base for the Cambrian Series 3, but recent studies have proposed new species without revising previously established ones. This paper offers a morphological statistical analysis based on both linear measurement and landmark-based geometric morphometric approaches performed on the earliest paradoxinine trilobites sampled in the Anti-Atlas (Morocco) and the Iberian Chains (Spain). As a result, the diagnosis of *Acadoparadoxides mureroensis* is emended and several species recently erected in Morocco (*A.* cf. *mureroensis*, *A. levisettii*, *A. ovatopyge* and *A. pampalius*) are suggested as synonyms of *A. mureroensis* until 3D statistical analyses are available based on material preserved on carbonate or silica nodules. The first appearance of *A. mureroensis* in both areas can be provisionally used for regional correlation until homotaxic tests are checked.

Keywords: systematics, biostratigraphy, Anti-Atlas, Iberian Chains, Gondwana

1. Introduction

Cambrian trilobites show higher levels of intraspecific variation than those documented in Ordovician–Permian taxa (Foote, 1991; Hughes, 1991, 1994; Jell & Hughes, 1997; Webster, 2007). In some cases, such as the correlation of the Cambrian Series 2–3 (or 'lower–middle Cambrian') boundary in the western Mediterranean region, the lack of biometrical analyses constraining the limits of diagnostic characters is preventing their application in biostratigraphy. If the diagnosis of new species is based on few specimens, the taxonomic validity can be highly uncertain. One solution to these problems is the splitting of trilobite taxonomy (see criticism in Rasetti, 1948; Hughes, 1994), but the lack of consideration of intraspecific variation is leading to the erection of parallel chronostratigraphic charts bearing similar species only distinguishable by overlapping mosaics of characters (Geyer & Vincent, 2014).

The paradoxidid trilobites represent one exemplary case of taxonomic splitting in Gondwana, Baltica and the Siberian Platform. Although the number of species has continued to increase in recent years and *c.* 150 species and subspecies have so far been erected (updated from Geyer & Landing, 2001, p. 124), few studies deal with their intraspecific variation (Bergström & Levi-Setti, 1978; Esteve, 2014). The criteria followed to erect species, lack of biometrical analysis and detailed comparisons in the paradoxidids directly affect

the validity of correlation of the traditional 'lower–middle Cambrian' (or Cambrian Series 2–3) transition in West Gondwana.

In the 1880s, the paradigm to recognize the lower–middle Cambrian boundary was mainly based on Brøgger's trilobite-based chronostratigraphic sketch (Brøgger, 1879, pp. 35–6; 1886), in which the olenellids were overlain by the paradoxidids with no overlapping. This sketch was based on Scandinavian evidence and was challenged by Hupé (1953), who pointed out the co-occurrence of olenellids and paradoxidids in the same strata of the central Anti-Atlas. A part of the regional 'Aguilizian' Stage (Hupé, 1960) and the 'Ouriken n'Ourmast horizon' (Choubert, 1963) was marked by a stratigraphic level, 50–60 m thick, with contemporaneous olenellids, protolenids and paradoxidids, resting with slight angular discordance on the basement (representing at present the Asrir/Brèche à Micmacca lithostratigraphic contact; see Álvaro *et al.* 2014). Hupé's basal horizon of the traditional middle Cambrian (Acadian) was located at the co-occurrence of these three trilobite families.

In the Iberian Chains of NE Iberia, Lotze (1961) characterized the 16–18 Band and Sdzuy (1961, 1971*a*,*b*) the Bilbilian Stage as a latest early Cambrian trilobite assemblage of protolenids, ellipsocephalids and redlichiids (without olenellids), found above a sandstone package (Daroca Formation) similar to the Moroccan Asrir Formation and below the first occurrence of paradoxidids. The Iberian lower–middle Cambrian boundary was tentatively located across a fossiliferous shale-dominated unit, named

†Author for correspondence: jj.alvaro@csic.es

informally the 'Ci/m' (lower–middle Cambrian transitional series) zone, with its base marked by the first appearance datum (FAD) of the trilobite *Acadoparadoxides mureroensis*. Sdzuy (1971*a*) correlated the Bilbilian with the uppermost Tasousekht substage (with doubts) and the Aguiliz substage of Morocco (Hupé, 1953, 1960). Neither Hupé nor Sdzuy rejected the possible diachronism on the FAD of paradoxidid trilobites throughout the Acado-Baltic Province (*sensu* Sdzuy, 1972) and suggested an unavoidable diachroneity of the FAD of their involved species. When Sdzuy (1971*b*) tentatively placed the FAD of *A. mureroensis* as a possible base for the middle Cambrian, he even assumed that this boundary could change in the near future.

During the last 30 years, the regional lower–middle Cambrian boundaries in Iberia and Morocco have evolved differently. In Iberia, the FAD of *A. mureroensis* has been maintained as the basal horizon of the middle Cambrian, whereas in Morocco another Cambrian chronostratigraphic subdivision has been proposed to replace Hupé's (1953, pp. 79–83) chart (Geyer, 1990; Geyer & Landing, 1995, 2004), and the new regional boundary is placed at the FAD of the genus *Hupeolenus* in the Asrir Formation.

Recently, Geyer & Vincent (2014) described the earliest paradoxidid trilobites that characterize Hupé's basal middle Cambrian mixture of olenellids, protolenids and paradoxidids in the Brèche à Micmacca Member. The authors proposed: (1) the record of eight paradoxidine species showing partial overlapping stratigraphic ranges in 12 m of the Tarhoucht quarries in the central Anti-Atlas; and (2) to refer the Iberian material of *A. mureroensis* (excepting the holotype) to *A.* cf. *mureroensis* on account of the poor preservation of the holotype (a cranidium described by Sdzuy, 1958). However, some of the species erected by Geyer & Vincent (2014) (i.e. *A. levisettii*, *A. ovatopyge* and *A. pampalius*) co-occurred in a single horizon of the Brèche à Micmacca at the Assemame quarry in the central Anti-Atlas (Zamora *et al.* 2014), which raised the question whether their supposed taxonomic distinctions are merely a matter of variation in a single species and questioned the correlation of their stratigraphic ranges throughout the Anti-Atlas. As the earliest paradoxidids from the Iberian Chains are characterized by a broad morphological variation and were grouped in a single species (*A. mureroensis*), which contrasts with the lack of morphological variation recognized within the Moroccan species by Geyer & Vincent (2014), a comparison between the Moroccan and Spanish species based on similar biometrical tests seems necessary to solve this taxonomic puzzle. The use of morphometrics in the analysis of those specimens provides an opportunity to quantify the intraspecific and biogeographical variation displayed by the earliest paradoxidine trilobites throughout the western Mediterranean region. This will allow a clear distinction among the diagnostic characters that differentiate these chronostratigraphic markers of the regional lower–middle Cambrian boundary intervals in Iberia and Morocco.

2. Geological setting and stratigraphy

Relics of the Cambrian in West Gondwana are disconnected throughout the western Mediterranean region and enclosed within Variscan and Alpine ranges, such as the Iberian Chains in Spain and the Anti-Atlas ranges in Morocco (Fig. 1). Recent palaeogeographic reconstructions point to the onset of a major Cambrian rifting axis connecting the Atlas and Ossa-Morena Rifts, flanked by a broad area subjected to extension that behaved like passive-margin platforms (e.g. the Cantabro-Iberian Basin where the Iberian Platform lies; for a recent synthesis; see Álvaro *et al.* 2014).

In the western Mediterranean region the immigration of paradoxidids is a key palaeoecological event that has been traditionally used for chronostratigraphic purposes (Álvaro *et al.* 1993, 2003; Liñán, Perejón & Sdzuy, 1993; Geyer & Vincent, 2014). In the Anti-Atlas, this immigration event is recognized in the *Morocconus notabilis* Zone (Geyer & Landing, 1995, pp. 37–40; *Morocconus* after Özdikmen, 2009) of the Brèche à Micmacca Member, which forms the lower part of the Jbel Wawrmast Formation (Destombes, Hollard & Willefert, 1985), a senior synonym of the Tamanart Formation *sensu* Geyer (1989). The formation is up to 300 m thick and classically subdivided into the Brèche à Micmacca and Tarhoucht members (Bondon & Neltner, 1933; Geyer & Landing, 2006). The former, up to 60 m thick, is composed of variegated volcano-bioclastic limestones, shales and subsidiary conglomerates. K-bentonites, lava flows and volcanosedimentary aprons form the base of the member in some areas of the Jbel Saghro region. The stratotype of the member is situated at Ourika Wawrmast. In the vicinity of Alnif (Assemame quarry; see below), a 'hot spot' of fossil echinoderm diversity has been reported (Smith, Zamora & Álvaro, 2013; Clausen, Álvaro & Zamora, 2014), which includes other skeletal remains, such as trilobites, brachiopods, skeletonized microfossils, hyoliths, molluscs, chancelloriids and reworked archaeocyaths (Buggisch, Marzela & Hügel, 1978; Geyer & Landing, 1995, pp. 47–120; Álvaro & Clausen, 2005, 2006, 2008; Clausen & Smith, 2008). The mélange of fossils from different biozones (including reworked archaeocyaths), displaying different diagenetic processes and the microstratigraphic subdivision of the carbonates punctuated by microbial crusts, led Álvaro & Clausen (2005, 2006, 2008), Álvaro (2014) and Álvaro *et al.* (2015) to recognize these volcano-bioclastic limestone interbeds as hiatal shell accumulations including allochems from different biozones. These condensed limestone interbeds are therefore inadequate for detailed biostratigraphic analysis, which contrasts with the continuous (unconformity-free) sedimentation recorded in the shale background deposition of the member. Despite
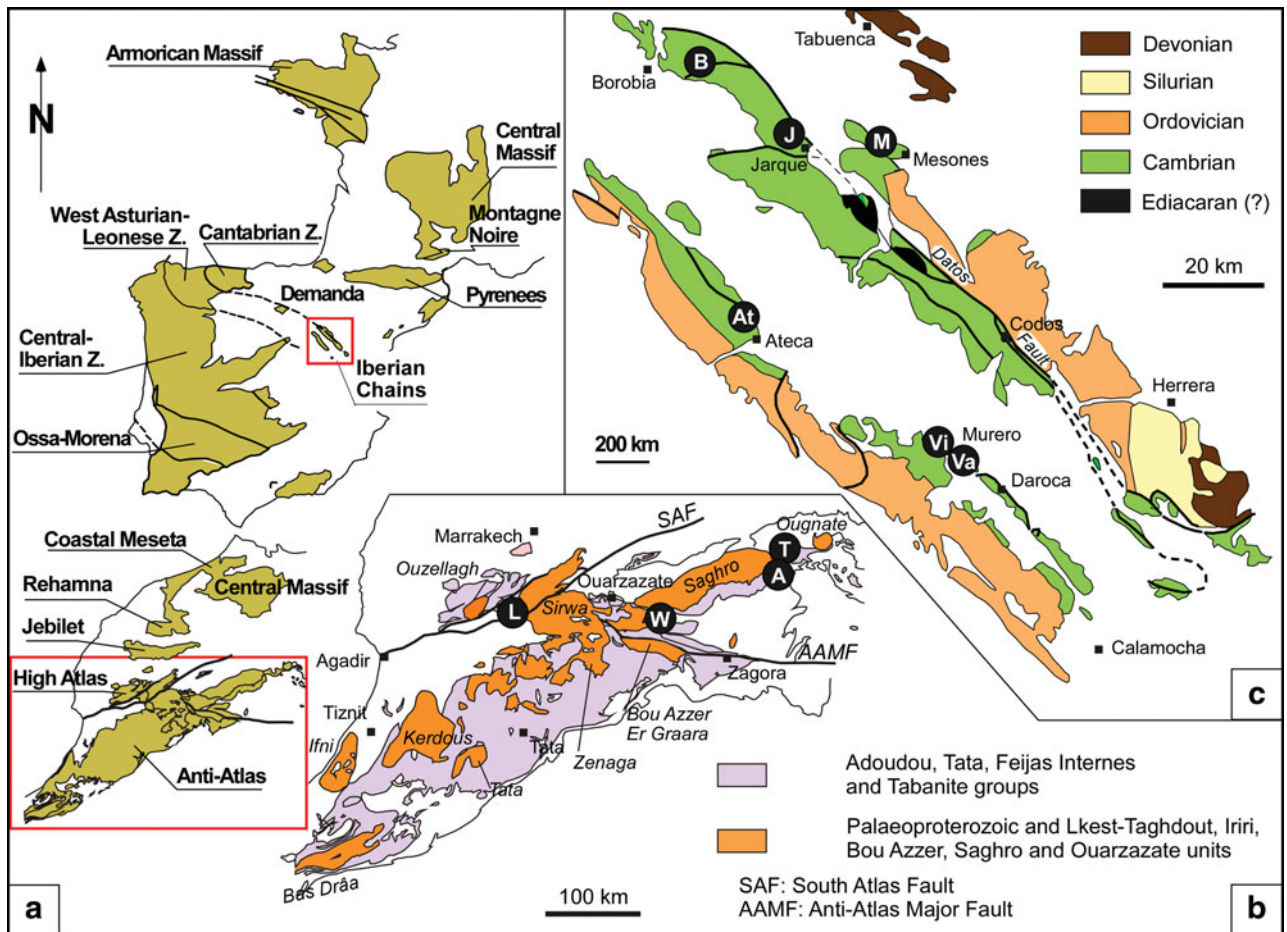
Figure 1. (Colour online) Geological and stratigraphic framework. (a) Pre-Variscan exposures of SW Europe and NW Africa, with detail of boxed areas in (b) High Atlas and Anti-Atlas Ranges, Morocco, and (c) Iberian Chains, NE Spain. Abbreviations of sections reported in the text: A – Assemame quarry; At – Ateca; B – Borobia; J – Jarque; L – Lemdad valley; M – Mesones; S – San Martín; T – Tarhoucht quarries; Va – Valdemiedes (Murero); Vi – Villafeliche; W – Ourika Wawrmast; and Z.– Zone.

some distinct diachroneities marking the base and top of the member, its sedimentation broadly took place in the *Morocconus notabilis* Zone. Finally, the 100–300 m thick Tarhoucht Member (traditional 'Schistes à *Paradoxides*') is a coarsening-upward shale-dominated unit punctuated by whitish bioclastic limestones and ash levels, the latter giving a variegated aspect to the host shale. The top of the member ranges from the *Morocconus notabilis* Zone to, at least, the *Kymataspis arenosa* Zone (Geyer & Landing, 1995, pp. 37–40).

In the Iberian Peninsula, the immigration of paradoxidids marks the Bilbilian–Leonian boundary (Gozalo *et al.* 2007). This lies in the Valdemiedes Formation, which consists of an alternation of green marly shales and carbonates, 20–150 m thick. The carbonate interbeds, both stromatolitic and bioclastic in character, comprise several facies associations, e.g. peritidal stromatolitic carbonate/shale couplets, shallow subtidal sponge-rich limestone/shale couplets, storm-induced bioclastic limestones, and open-platform offshore-dominated shales (Álvaro & Vennin, 1997). In the Villafeliche graben (where the Valdemiedes stratotype lies), this interval is composed of offshore-dominated shales; the palaeogeographic position of this graben (surrounded by shallower deposits) suggests that the sea floor was becoming differentiated into a mosaic of topographic highs and lows. The sedimentation of the Valdemiedes Formation was controlled by the interplay of two variable factors: an episodic tectonic activity (Álvaro & Vennin, 1996) and a cyclic Milankovitch-like orbital forcing (Álvaro *et al.* 2000). A quantitative analysis of the tectonically induced subsidence recorded in the Iberian platform revealed a distinct tectonic disturbance at the Bilbilian–Leonian boundary associated with further minor pulses. The successive tectonically induced disturbances produced a major rearrangement in the intra-platform patterns of differential subsidence, in which the so-called Villafeliche graben can be considered as the hinge point of geodynamic rearrangement. The FAD of *A. mureroensis* marks the top of the so-called Valdemiedes event, which was interpreted by Álvaro & Vennin (1997) and Clausen & Álvaro (2002) as the end of one shallowing-upward cycle (0.4–3.4 m thick) and a community turnover or replacement, recorded in mixed substrates of the Iberian platform (Álvaro *et al.* 2000). This shallowing was recorded under shoreface conditions in central parts of the platform (e.g. Jarque and Mesones sections), offshore conditions under clayey sedimentation in the Villafeliche
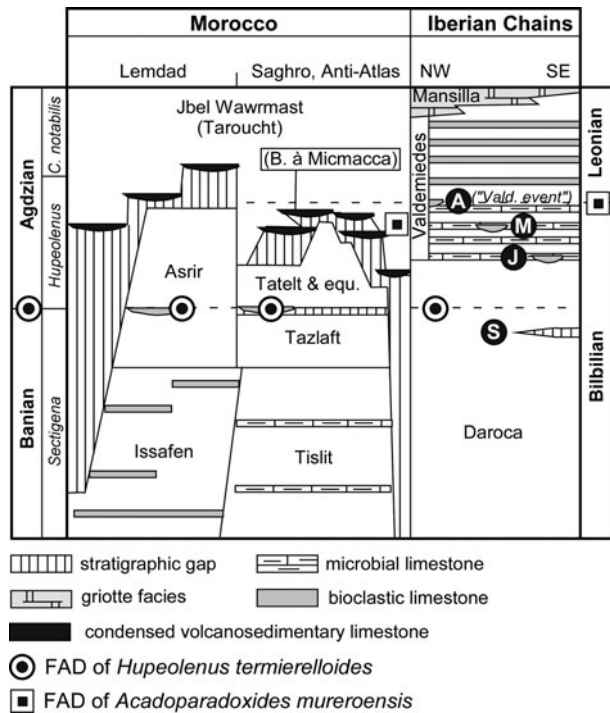
Figure 2. Stratigraphic logs of the regional lower–middle Cambrian transition in the Anti-Atlas and Iberian Chains; modified from Álvaro (1994) and Álvaro *et al*. (1993, 2014). Localities from the Iberian Chains are At – Ateca, J – Jarque, M – Mesones and S – San Martín (see their geographical setting in Fig. 1).

graben (Valdemiedes section) and condensed, amalgamated, tempestite accumulations in distal parts of the platform (Ateca section; Fig. 1). The top of the event is capped by flooding conditions (marking the beginning of the following shallowing-upward cycle) that recorded the immigration of new trilobite families (e.g. paradoxidids in the *A. mureroensis* Zone). Successive cycles recorded in the Valdemiedes Formation allowed a stepwise immigration of new invaders (including conocoryphids and acrocephalitids), leading to a progressive increase in biodiversity.

3. Material and methods

A new sampling of trilobites across the Iberian concept of the lower–middle Cambrian boundary interval was necessary in the Anti-Atlas controlling the stratigraphic ranges of each trilobite species. We selected the Assemame open quarry (property of Moujan family, Ksar Timrzite in Alnif, Morocco), in the vicinity of Alnif (31° 17.292′ N, 4° 59.156′ W), central Anti-Atlas, because the quarry comprises a complete section of the Asrir and Jbel Wawrmast formations. The Brèche à Micmacca Member, *c*. 35 m thick, is extremely fossiliferous, and its shale interbeds have yielded a rich fauna of complete and partly disarticulated echinoderms, trilobites, brachiopods and molluscs (Figs 2, 3). The 'telesto level' is commonly used by amateur palaeontologists to recognize a kind of 'acmé level' of *Cambropallas telesto* Geyer, 1993. The level is currently recognized in the *Morocconus not-*

abilis Zone. The interest of the Assemame quarry is threefold: (i) sampling of slightly deformed trilobites in shales allowing a taxonomic comparison with moderately to strongly deformed specimens from the type locality in the Iberian Chains; (ii) a biogeographical comparison with other known fossiliferous logs of the Anti-Atlas (e.g. the Tarhoucht open quarry; Geyer & Vincent, 2014) and the Iberian Chains (e.g. Murero; Liñán & Gozalo, 1986); and (iii) identification of the FAD of paradoxidids different from the classical ones, such as the Ourika Wawrmast stratotype (Hupé, 1953) and the Tarhoucht quarries (Geyer & Vincent, 2014). The lower 10 m of the Brèche à Micmacca Member offers a key section of fossiliferous shale interbeds in non-condensed, offshore-dominated, clayey substrates representative of the middle part of the *M. notabilis* Zone. Most of the sampled trilobites and echinoderms are complete or with low degree of disarticulation, and suggest that the fauna from the shale interbeds of the Assemame quarry represents autochthonous and parautochthonous fossil assemblages. The material described below has been sampled by the authors in a shale interbed (30 cm thick) of the Brèche à Micmacca Member exposed in the Assemame open quarry, central Anti-Atlas (see log and stratigraphic ranges of reported fossils in Fig. 3).

The morphometric analyses documented below are based on: (1) 16 pygidia and 13 cranidia sampled in the Assemame quarry by the authors; (2) 6 cranidia and 10 pygidia of *A*. cf. *mureroensis*, 9 cranidia and 13 pygidia of *A. pampalius*, 23 cranidia and 20 pygidia of *A. levisettii*, 1 cranidium and 4 pygidia of *A. nobilis*, and 7 cranidia and 8 pygidia of *A. ovatopyge* from the Tarhoucht quarries of the central Anti-Atlas (MMUW, Naturmuseum Senckenberg, Frankfurt), reported by Geyer & Vincent (2014); and (3) the type material of *A. mureroensis* (Sdzuy, 1958; PIW, Naturmuseum Senckenberg, Frankfurt) supplemented by 13 cranidia and 7 pygidia of the same species from the type locality (MPZ, Museo de Ciencias Naturales of the Zaragoza University).

Figure 4 and Table 1 show the linear measurements and abbreviations used for cranidial and pygidial statistical analysis. Linear measurements were made using ImageJ software (Abràmoff, Magalhães & Ram, 2004), which allows measurements of continuous variables, such as the palpebral lobe or preglabellar field lengths. Bivariate analyses were calculated using the reduced major axis (RMA) approach based on log10 transformations of original linear dimensions. The analyses were carried out using the PAST software package (Hammer & Harper, 2006). This software provides error estimates that can be calculated with two methods: standard linear regression approximations and bootstrapping over cases. The bootstrap resampling was completed 1000 times in each case to permit the calculation of confidence intervals for both the slope and interception in each RMA. For a synoptic view of some results obtained with RMA, a principal component analysis (PCA) was performed using the
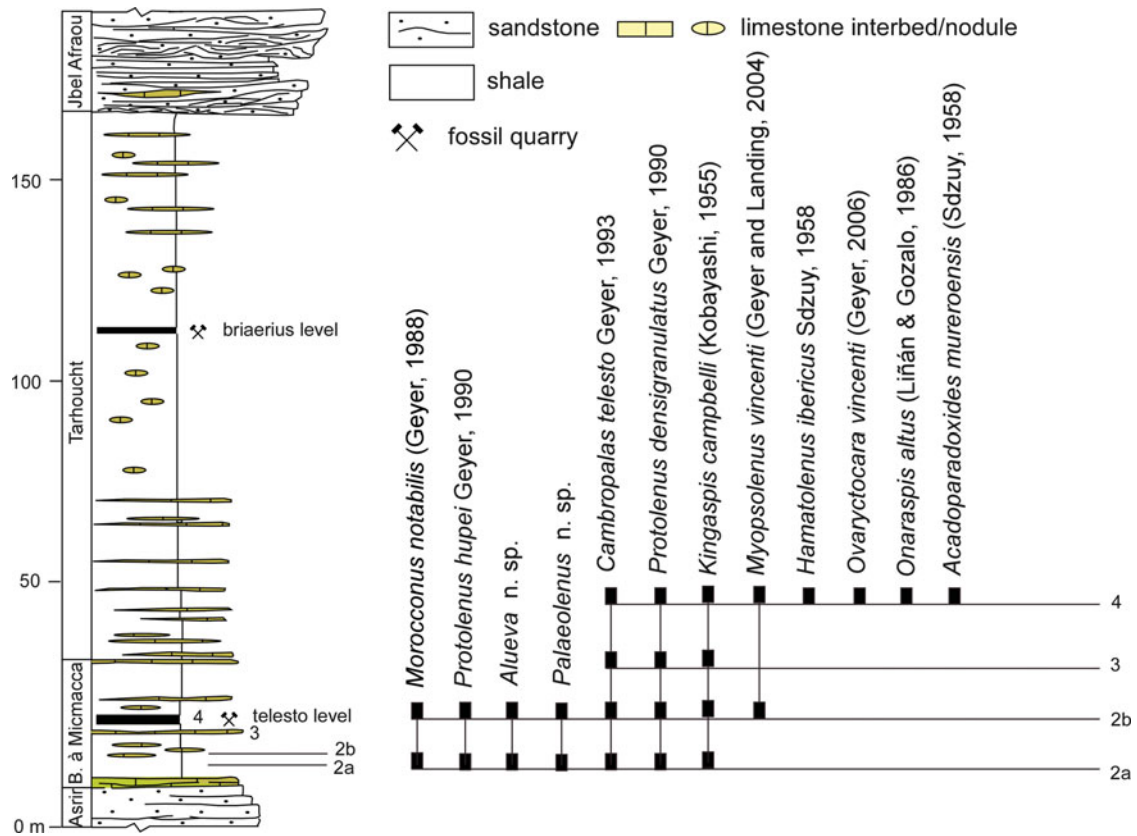
Figure 3. (Colour online) Stratigraphic ranges of trilobites described in the text from the Assemame quarry, central Anti-Atlas; modified from Zamora *et al*. (2014).

Table 1. Abbreviations used in the text for trilobite sclerite dimensions

Cranidium	
Lc	Length of cranidium (sag.)
Lg	Length of glabella (sag.)
Lab	Length of anterior border of cephalon (sag.)
Lpf	Length of preglabellar field (sag.)
Ler	Length of eye ridge (exsag.)
Lpl	Length of palpebral lobe (exsag.)
LOr	Length of occipital ring
Wp	Posterior glabellar width (tr.)
Wa	Anterior glabellar width (tr.)
Wcp	Width of cranidium across palpebral lobes.
Faw	Frontal area width (tr.)
Pbw	Posterior border width (tr.)
Pygidium	
Sl	Sagittal length
Al	Axis length (rachis)
Aw	Anterior width
Mw	Maximum width

PAST software package. PCA also helps to examine the effects of deformation in specimens from a single bed (=same population) (Hughes & Jell, 1992; Esteve, 2014).

Taking into consideration the subtle differences in the cranidial and pygidial shapes of these trilobites, characterized by a simple Bauplan, some morphological differences cannot be recovered by simple bivariate and multivariate analyses. Therefore, a complementary quantification of morphological variation was assessed using geometric morphometric methods

(Bookstein, 1991; Zelditch *et al.* 2012). Landmarks and semi-landmarks were digitized from pictures using the software TpsDig v.2.16 (Rohlf, 1990). A total of 30 landmarks (four along the sagittal axis and 13 pairs on either side of the axis) were chosen to represent the overall shape of the cranidium (Fig. 4a, b), and 11 landmarks (five along the sagittal axis and three pairs on either side of the axis) and 150 semi-landmarks were selected to represent the overall shape of the pygidium (Fig. 4c, d). As the trilobites have bilateral symmetry, we selected half of the landmarks and semi-landmarks from one side (left or right). This procedure allowed analysis of more specimens because even some incomplete specimens could be used for morphometric analysis. The landmarks and semi-landmarks of each specimen were used for statistical analysis and graphic illustration. The data were exported directly to IMP software (Sheets, 2014) for statistical treatment of a set of landmark coordinates (x, y). In order to standardize the size, orientation and position of each specimen (and thus the alignment of each landmark), a Procrustes superimposition of data was applied before analytical processing (the resulting coordinates are named, after fitting, Procrustes coordinates). Coordinates of semi-landmarks were calculated from the outline data in SemiLand8 (Sheets, 2014) using the minimized Procrustes distance method to optimize their location along the outline. All statistical analyses were performed using warp scores, which are derived from thin-plate spline decomposition (Rohlf,
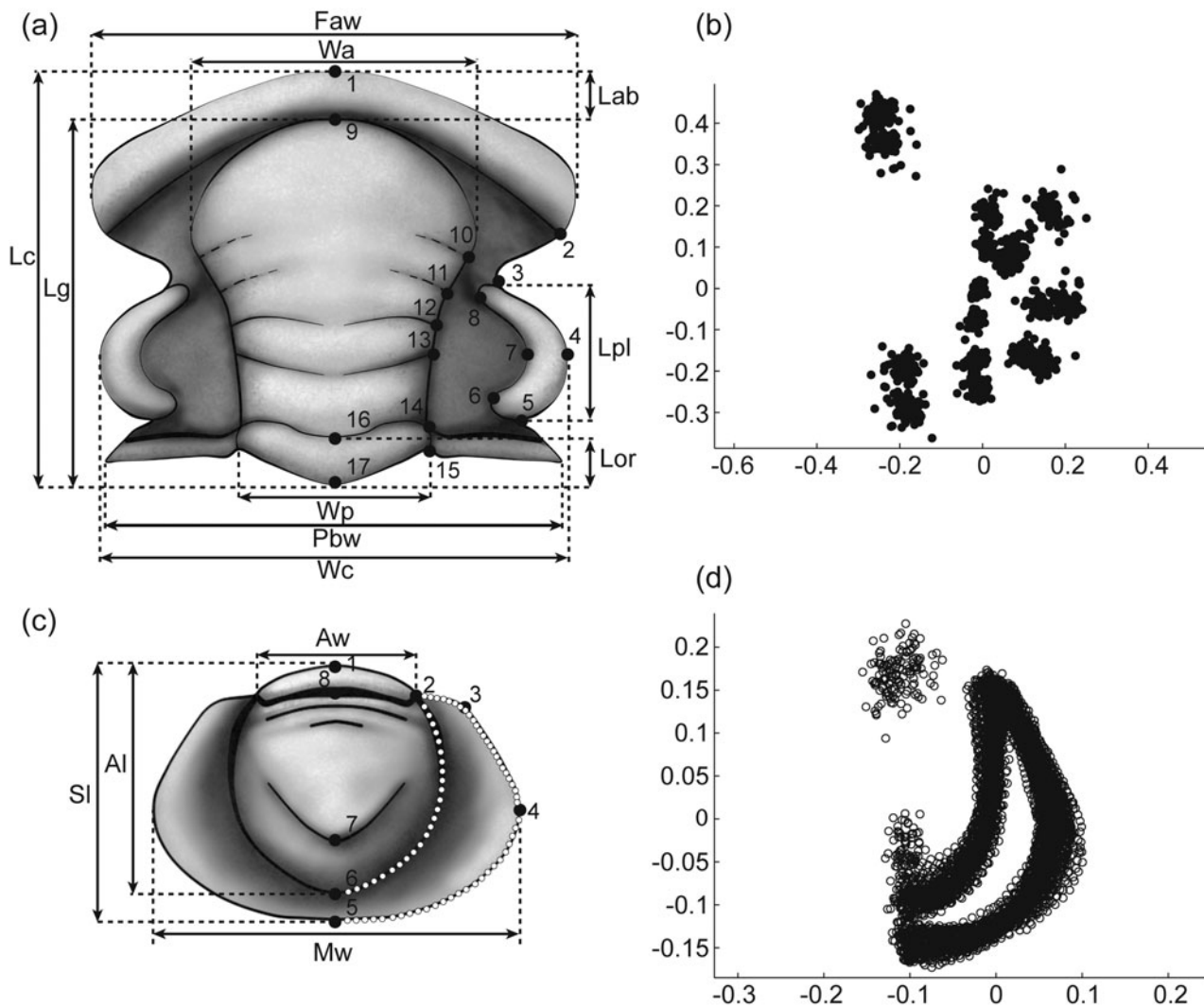
Figure 4. Reconstruction of *Acadoparadoxides mureroensis* (Sdzuy, 1958) with abbreviations used in the text, statistical analyses, landmark (black circles) and semi-landmark (white circles) configuration. (a) Cranidium (see abbreviations in Table 1). (b) Superimposition plot of cranidial landmark data. (c) Pygidium (see abbreviations in Table 1). (d) Superimposition plot of pygidial semi-landmark data.

1990; Bookstein, 1991; Zelditch *et al.* 2012). Variation within and between samples was visually compared using PCA of the warp scores. An analysis of canonical variates of the warp scores and a bootstrapped F-test of Procrustes coordinates were used to test the significant morphological differences between samples (Webster & Sheets, 2010; Zelditch *et al.* 2012). We used a bootstrapped F-test because it does not assume any isotropic normal distribution of landmarks around the mean; visual inspection of the variation around each landmark after Procrustes superimposition (Fig. 4b, d) indicates that such an assumption is not reached by these data. In order to compensate for the multiple comparisons made using the bootstrapped F-test, we applied a Bonferroni correction to the critical *p*-value. The degree of variation in each sample was measured as within-group variance in Procrustes distance away from the group mean. In order to test the difference of all multivariate samples, we also carried out a multivariate analysis of variance (MANOVA) and

a canonical variates analysis (CVA). The latter provide a scatter plot of specimens along the two first (the more representative; Mardia, Kent & Bibbly, 1994) canonical axes, producing maximal and second to maximal separation between all groups (multigroup discriminant analysis).

3.a. Retrodeformation techniques

The Moroccan and Iberian specimens show different degrees of flattening and tectonic distortion. The specimens from the Spanish-type locality (Murero) commonly display higher degrees of deformation (Liñán & Gozalo, 1986) than the Moroccan ones, and this has been used to question the validity of *Acadoparadoxides mureroensis* (Geyer & Vincent, 2014). Many techniques have been described for the restoration of deformed fossils, especially in trilobites: e.g. Sdzuy (1966), Cooper (1970), Briggs & Williams (1981), Jefferies, Lewis & Donovan, (1987), Cooper (1990),

Hughes & Rushton (1990) and Hughes & Jell (1992). Some of them reconstruct the strain ellipse based on either deformed right angles of several specimens preserved on the same slab or orientating the specimens in relation to the direction of greatest stress (Cooper, 1990), whereas others restore the vertical component of deformation after comparing with putatively undeformed specimens from other outcrops (Kim, Sheets & Mitchell, 2009). In our case study, due to the lack of several specimens lying on a single slab and displaying different orientations, and the absence of distinct traces of penetrative cleavage associated with the analysed specimens, we follow Hughes & Jell (1992) and Srivastava & Shah's (2006) method based on the manipulation of digital images with Adobe Photoshop CS5: rotating the image until the posterior margin of the cranidium is horizontal and then skewing the image horizontally to restore bilateral symmetry, bringing the sagittal axis to vertical. All the analysed specimens represent mature forms.

The distortion of the specimens analysed in this work was assessed with the above-reported bivariate and multivariate methods, whereas the geometric morphometric method assessed the overall intraspecific variation in cranidia and pygidia. The correlation coefficients of perpendicular linear measurements obtained with RMA provide useful insights about the variation controlled by distortion: lower correlation coefficients ($r < 0.7$; see below) suggest high dispersion patterns of data reflecting the influence of both compaction and shearing, whereas higher correlation coefficents ($r > 0.8$) suggest a negligible influence in the shape. As documented below, some bivariate plots show greater dispersions of data when comparing length-to-width ratios than length-to-length ratios, but r is always >0.9, so isometric/allometric growths cannot be biased by deformation in our analyses. In addition, wide scatters also indicate that some characters have more flexible growth controls than others (Labandeira & Hughes, 1994, p. 493); as a result, these controls are tested with PCA scores. The results show that, despite tectonic distortion, the general shape of the whole sample and the ratios of parallel measurements are maintained.

4. Former diagnostic characters of *Acadoparadoxides* species from the Mediterranean region

Acadoparadoxides mureroensis, whose FAD traditionally marks the base of the regional middle Cambrian (Leonian Stage) in Spain, has been (and still is) a source of controversy. It has been reported from Spain, Morocco, Turkey, Sardinia and Poland. Based on disputed synonymies, Gozalo *et al*. (2013, p. 147) also reported this taxon in Siberia (= *A. eopinus*) and Avalonia (= *A. harlani*). Geyer & Vincent (2014, pp. 47–8) considered the type cranidium as too distorted to be properly identified outside the type locality and referred similar material from the rest of Spain and Morocco to *A*. cf. *mureroensis*. However, des-

pite the obvious compaction- and tectonic-related deformation of the Iberian material, many studies (e.g. Hughes & Rushton, 1990; Hughes & Jell, 1992, 1999; Jell & Hughes, 1997; Webster & Hughes, 1999; Peng *et al*. 2015) have demonstrated that, having a large set of specimens from the same interval, the preservation of trilobites does not preclude confident determinations. Based on material from the Tarhoucht quarries, Geyer & Vincent (2014) proposed a phylogenetic scenario with overlapping replacement of several species of *Acadoparadoxides* throughout the lowest few metres of the Brèche à Micmacca Member. However, this phylogenetic hypothesis focused on pygidial modifications was not supported by biometrical analyses. The authors found a stratigraphic succession of species exhibiting slight changes in the pygidium, such as the anterior and posterior widths and the relative length of the axis (Geyer & Vincent, 2014, fig. 13). When Zamora *et al*. (2014) reported many of Geyer and Vincent's species from a single horizon of the neighbouring Assemame quarry, this phylogenetic hypothesis was called into question and opened new options, e.g. does *Acadoparadoxides* display such a morphological variation in the beginning of the mid Cambrian? Or do Geyer and Vincent's species represent a single species with infraspecific variants grading into each other? Similar changes in the pygidium of *A. mureroensis* and other paradoxidid trilobites from Spain were reported by Gozalo, Liñán & Díes (2003), but their interpretation exclusively dealt with intraspecific dimorphism, a hypothesis that is checked below. Esteve (2014) documented how such variations in the pygidium of other paradoxinines (i.e. *Eccaparadoxides pradoanus*) show a continuous spectrum, as a result of which intraspecific variation is related to morphological (size-dependent vs not size-dependent) rather than dimorphic variation.

The erection of new Moroccan and Turkish species of *Acadoparadoxides* close to the Iberian lower–middle Cambrian boundary interval in the Mediterranean region has been based on the following characters:

(1) *Paradoxides* (*Acadoparadoxides*) *nobilis* Geyer, 1998 (p. 387) was originally distinguished from *A. mureroensis* by 'a flattened surface of both anterior and anterolateral borders and also of the central areas of the palpebral lobes' (vs slightly convex in the latter); 'the posterior margin of the hypostome is curved' (vs an almost straight median part); 'pygidium with a slightly longitudinal triangular shape with rounded posterolateral corners and a faintly indented posterior border' (vs a relatively rounded posterior margin, which may at best attain a nearly straight posterior medium part of this margin); 'pygidial rachis is less clearly defined [in *A. mureroensis*], which also has one quite well-defined axial ring'; 'the true axis ranges between 60–75 % of the pygidial length' (vs 72–82 %). However, the cranidia illustrated by Geyer (1998) offered some doubts, as neither the holotype (pl. 1, fig. 6) nor the figured paratypes (pl. 1, figs 11–12; pl. 3, fig. 5 was a

juvenile and incomplete specimen) are complete, as a result of which the total length of the cranidium and the relative longitudinal proportions of other characters were necessarily estimated and not directly measured. The relative convexity of the anterior and anterolateral borders does not differ from other Spanish specimens also preserved in shales, but distinctly differs from specimens preserved in limestones (Álvaro, 2007, fig. 4k). No complete specimens were illustrated, so both the hypostoma and pygidia should be considered as tentatively assigned to this species.

Subsequently, Geyer & Vincent (2014) offered another mosaic of characters to differentiate both species although, as in the previous paper, complete specimens were still absent and their cranidia fragmented: specimens illustrated in their fig. 25a, b, d show cranidia with broken anterior borders, and their fig. 25n is the only cranidium that allows a complete biometry. Its table summary (fig. 12) offered some slight differences between *mureroensis* and *nobilis*, such as a frontal lobe of the glabella 1.27–1.44 vs 1.36–1.44 times (so overlapping ranges) the width of the occipital ring, respectively; eye lobes 35–43 % vs 38–44 % of cranidial length (also overlapping values); anterior margin 'evenly curved to subarcuate' vs 'evenly curved' (partly coinciding shapes); dorsal face of anterior border 'convex' vs 'distinctly flattened' (a character strongly controlled by taphonomic conditions; see discussion below); a pygidial outline with posterior margin 'slightly rounded to almost straight' vs 'indented' and rachis 72–82 % (but 67 % in their fig. j) vs 62–74 % of pygidial length (again overlapping values; this latter character was used by Gozalo, Liñán & Díes (2003) to differentiate two morphotypes of *mureroensis*). In their discussion, the authors offered some 'significant criteria to unequivocally distinguish *nobilis* from cf. *mureroensis*', which are: (1) 'dorsal surface of the anterior border flattened rather than low and evenly convex', a character not reliable when comparing material preserved in shales (Geyer & Vincent, 2014, fig. 22e, g); (2) 'eye lobes bilobate, with flattened median dorsal surface', a character unseen both in the holotype of *nobilis*, due to its state of preservation, and the paratypes (Geyer, 1998, pl. 1, figs 6, 12–13), and only preserved in the right palpebral lobe of fig. 25d and the left one of fig. 25n (Geyer & Vincent, 2014); (3) 'posterior margin of hypostome gently curved rather than with faint curvature', a character that offers no distinct differences; (4) 'a pygidial outline longitudinally triangular with gently curved posterolateral corners', a character shared by both species; and (5) a posterior margin of pygidium with slight median indentation rather than flat to slightly convex. *A priori*, this latter difference should be distinct enough to distinguish *mureroensis* from *nobilis*.

(2) *A. pampalius* Geyer & Vincent, 2014 and *A. levisettii* Geyer & Vincent, 2014 are two species erected in the Bou Tiouit section. Their cranidial differences are: (1) the width of the frontal lobe in comparison with the occipital ring: 1.33–1.45 in *pampalius*, 1.26–1.41 in *levisettii* and 1.27–1.44 in cf. *mureroensis* (an overlapping value); and (2) the cranidial (tr.) 'width between the suture at the anterior border, which equals the transverse width across the eye lobes or is slightly smaller in *pampalius*, whereas the anterolateral corners in *levisettii* project beyond the level of the visual suture' (a character not shared by the cranidia of *pampalius* illustrated in fig. 14h–j and by those of *levisettii* in figs 18o and 19f, m). Their pygidial differences are: (1) pygidium sub-rounded to slightly subhexagonal in *pampalius*, subhexagonal to subtriangular in *levisettii* and subtriangular in *mureroensis*, so displaying gradual transitions; (2) rachis 55–60 % (but 64 % in the holotype; fig. 16a), 60–68 % and 72–82 % of pygidial length, respectively; and (3) terminal axial piece narrowly rounded in the two former and subacute in the latter (another character showing broad gradation). As a result, the only difference between *pampalius/levisettii* and *mureroensis* is the concave base of the pygidial pleurae and posteroaxial area forming a slight bowl-shaped depression, whereas in *mureroensis* this area would be broadly flat.

(3) *A. ovatopyge* Geyer & Vincent, 2014 was another species erected from the Bou Tiouit section. According to the authors, the cranidium of this species differs from *A.* cf. *mureroensis*: (1) in the glabellar shape, subparallel vs slightly expanding at L1–L2 (a character not distinguishable when comparing populations of *A. ovatopyge* and *A. mureroensis*); (2) glabellar frontal lobe, 1.27–1.44 vs 1.34–1.45 times (overlapping values) the width of the occipital ring; (3) relative length of the palpebral lobe, 35–43 % vs 34–41 % of cranidial length (overlapping values); (4) anterior margin of the cranidium, evenly curved to subarcuate vs slightly subarcuate (partly coinciding); and (5) anterior border convex vs flattened (a character potentially masked by taphonomy), respectively. The only significant difference yielded by Geyer & Vincent is offered by comparisons of the pygidia: *mureroensis* would differ from *ovatopyge* in (1) the subtriangular (posterior margin slightly rounded to almost straight) vs ovate (occasionally slightly truncated); and (2) the 72–82 % vs 66–72 % of the relative (sag.) length of the rachis (again, Gozalo *et al.*'s character to distinguish two morphotypes of *mureroensis*), but see *ovatopyge* fig. 28b (Geyer & Vincent, 2014) with a ratio of 77 %. As stated by the authors (p. 56), the 'pygidia of *A. ovatopyge* are often also similar to those of *A.* cf. *mureroensis* and occasionally difficult to distinguish. However, differences in those similarly developed pygidia exist in the more subovate outline of the *A. ovatopyge* pygidium rather than a subelongate shape as in *A.* cf. *mureroensis*, and a slightly less raised and less clearly defined platform of the rachis, which extends closer to the posterior margin', both characters already discussed above. Therefore, differentiation between *A. ovatopyge* and *A. mureroensis* was very tenuous, and a statistical analysis seems necessary to assess these differences (see below).

(4) *Acadoparadoxides deani* Geyer & Vincent, 2014 (pp. 57–8) was erected to accommodate some paradoxidine specimens from SW Turkey assigned by Dean & Özgül (1994) to *A. mureroensis*. Geyer & Vincent (2014) differentiated the Turkish specimens from their *A. mureroensis* concept in having smaller size; slightly expanded glabella at L2, and slightly wider (1.35 times); glabellar frontal lobe less curved; wider (tr.) eye lobes of *c.* 11 % of cranidial width; narrow fixigenae of *c.* 16–18 % of cranidial width; S2 deep, slightly curved, more or less transverse lateral sections and a relatively short (tr.) and shallow median section; a faintly subarcuate anterior margin; an anterior border with uniformly low convexity; a fairly narrow (tr.) occipital ring (*c.* 49–51 % max. cranidial width) that extends considerably beyond the posterior border; a small occipital node located slightly posterior to mid-length of the occipital ring; a fairly elongate shape of the pygidium (width/length ratio *c.* 0.82); a slender rachis of *c.* 78 % of pygidial length; a fairly wide (tr.) articulating half-ring of the pygidium.

In our statistical analysis, we include all the above-reported species except *A. deani*, because the cranidia of the latter are incomplete and the specimens illustrated by Dean & Özgül (1994) cannot reliably be measured. The erection of *A. deani* seems premature because the incomplete cephala from Turkey share the diagnostic characters of *A. mureoensis*, and pygidia are poorly preserved. Complete and well-preserved specimens from Turkey are necessary before taking a definitive decision about the status of *A. deani*.

5. Morphological analysis

In order to assess whether *A. mureroensis* may be identified outside its type area (the Iberian Chains) and whether the species shows intraspecific dimorphism or high levels of variation, we carried out a morphological analysis based on all the specimens illustrated from Spain (including the type material), Geyer & Vincent's (2014) illustrated specimens from the Anti-Atlas, and new ones collected by us from the Assemame quarry. Although the specimens sampled in a single bed of the Assemame quarry can be assigned to various of Geyer & Vincent's species (see Zamora *et al.* 2014), we analyse them below as a single population. The aim of this method is to assess whether the Assemame population falls within the morphospace of a single Moroccan species or, on the contrary, its morphospace is shared by other species.

5.a. Cranidia

When comparing the species of *Acadoparadoxides*, many differences deal with some cranidial characters, such as the width of the glabellar frontal lobe (Wa in Fig. 4) vs the width of the occipital ring (Wp); and the width of the anterior border vs the width across the eye lobes, and the length of the palpebral lobe. Other differences between the species of *Acadoparadoxides*

are also related to the general shape of the glabella. The discrimination of these morphological characters and recognition of allometric trends in such characters can be assessed using bivariate and multivariate analyses. As stated above, the cranidial and pygidial shapes of this genus display subtle morphological variations, difficult to quantify with few variables. In order to improve the quantification of the *Acadoparadoxides* shape, we combine below the multivariate analyses with geometric morphometric methods. Measurements are summarized in Table 1.

(1) Bivariate analysis (RMA). The morphological differences of eight cranidial variables have been assessed with respect to a standard measure for cranidial size. The latter has been chosen as Lg because its axial features are relatively constant in trilobites (see Palmer, 1957; Hughes, 1994). Eight linear variables have been selected: four length measurements parallel to the sagittal axis, and four width measures orthogonal to it.

Length of anterior border (Lab). Figure 5a shows the relationship between Lab and Lg in all analysed specimens. RMA shows that the growth of Lab is negatively allometric with respect to Lg at the 95 % confidence level ($n = 70$, $a = 0.78$, $b = -0.63$, $r = 0.92$, $p < 0.0001$). Within the sample, the increase in Lab shows a considerable variation. This result suggests that Lab allometry is very strong.

Length of palpebral lobe (Lpl). Figure 5b shows the relationship between Lpl and Lg in all analysed specimens. The growth of Lpl with respect to Lg is negatively allometric at the 95 % confidence level ($n = 68$, $a = 0.85$, $b = -0.211$, $r = 0.98$, $p < 0.0001$).

Posterior and anterior glabellar widths (tr.) (Wp–Wa). The maximum Wp and Wa both vary with respect to Lg, indicating an isometric growth at the 95 % confidence level (Wp: $n = 71$, $a = 1.094$, $b = -0.399$, $r = 0.96$, $p < 0.0001$, Fig. 5c; Wa: $n = 70$, $a = 1.0875$, $b = -0.26$, $r = 0.96$, $p < 0.0001$, Fig. 5d). However, the bivariate plot shows a slight variation in both variables within the sample, especially among larger specimens. Although the standard error is quite small (std error at 0.034 for *a* and 0.032 for *b*), the 95 % bootstrapped confidence interval ($N = 1999$) is quite wide (*a*: 1.04, 1.151 and *b*: 1.024, 1.153). Because the specimens display tectonic deformation, in particular those from Murero, the widely dispersed values may reflect distortion, notably in the glabella, which is commonly flattened. Wp has also been assessed with reference to Pbw and shows an isometric growth at the 95 % confidence level ($n = 36$, $a = 1.061$, $b = 0.266$, $r = 0.99$, $p < 0.0001$). To check these results, a comparison between the regression coefficients of these variables was carried out based on a MANOVA (Wilk's lambda: 0.07006, df1: 2: df2: 64; F: 424.8; $p < 0.00001$). These results suggest that there is no significant variation in Wa and Wp within the sample.

Frontal area and posterior border widths (Faw – Pbw). Both widths vary with respect to Lg, indicating slight allometric growth patterns at the 95 %
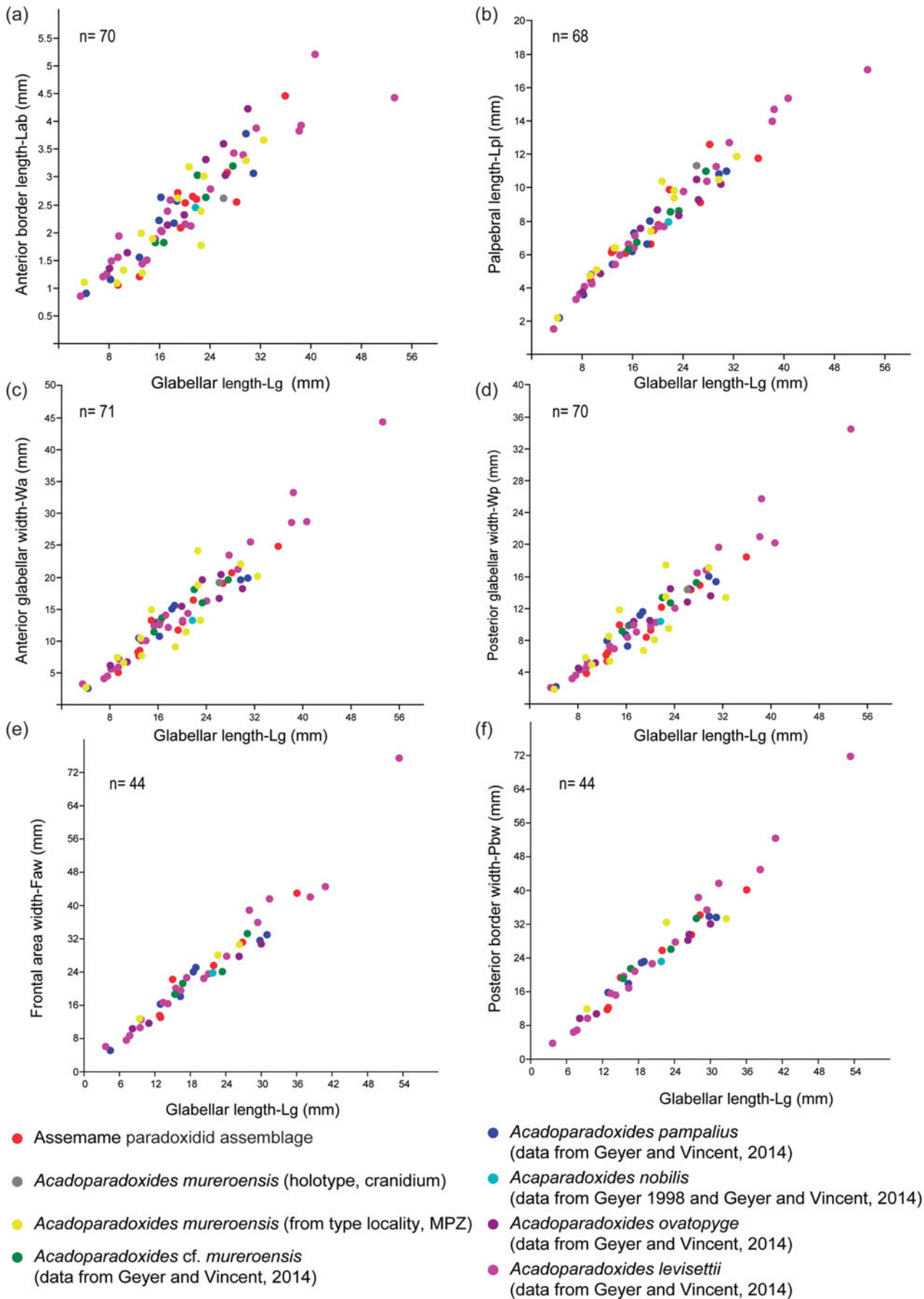
Figure 5. (Colour online) Bivariate plots showing relationship between glabellar length and anterior border length (a), palpebral lobe length (b), anterior glabellar width (c), posterior glabellar width (d), frontal area width (e) and posterior border width (f).

confidence level for the frontal area ($n = 44$, $a = 0.98$, $b = 0.097$, $r = 0.97$, $p < 0.0001$; Fig. 5e) and the posterior border ($n = 43$, $a = 1.1068$, $b = -0.07$, $r = 0.98$, $p < 0.0001$; Fig. 5f). There is a high variation in both variables within the sample. There is a strong correlation between the frontal area and Lg ($r = 0.97$, $n = 44$), and RMA shows an isometric growth in the sample at the 95 % confidence level. The correlation between the breadth of the posterior border and Lg is slightly higher ($r = 0.98$, $n = 43$) and RMA also shows isometric growth in the sample at the 95 % confidence level.

RMA shows that variations of some cranidial characters are size-independent. Growth patterns indicate that Lab and Lpl developed strongly allometrically, and the frontal area and posterior border widths developed more or less clearly allometrically. Only the posterior glabellar and maximum glabellar widths show an isometric growth. These allometric growths are responsible for changes in the general morphology of the cranidium. Appreciation of both allometric and isometric growths and of size-independent changes is important, as they show that the morphological variation within the sample suggests conspecific relationships. Although some morphological variations may be related to compaction-related deformation, the correlation of coefficients linking perpendicular linear measurements is high ($r > 0.96$). The Spanish specimens display more deformation features and their correlation coefficients are slightly lower for perpendicular measurements ($r \sim 0.9$). In any case, their compaction- and tectonic-related deformation does not preclude the correct identification of their general shape. Therefore, although the types from Murero are broadly distorted, this does not lead to taxonomic confusion and our material can be distinctly assigned, as well as the rest of the species studied here, to *A. mureroensis*.

(2) Multivariate analysis (PCA) of the cranidium. Although the bivariate analysis suggests that all the involved species belong to a single morphospecies, it is possible that (if viewed synoptically) multiple measurements could reveal the presence of separate clusters. Thus, a PCA was employed to test this possibility.

The analysis ($n = 53$) included five characters, three axial lengths (Lg, Lab and Lpl) and two transverse widths (Wp and Wa). In the second PCA ($n = 35$), we added two parameters: the frontal area and posterior border widths.

The eigenvalues (Table 2) show the degree of variation accounted for by each principal component. The contributions of each variable to each principal component have also been calculated as the eigenweights or scores (Table 2). The first and second components account for most of the variation within the sample in using correlation and variance–covariance matrixes (94.008 % and 97.494 %, respectively). All variables have positive eigenvalues, and eigenweights are comparable among all variables (Table 2). Similar loadings for the first component suggest that PC1 reflects the overall size of the specimens, which accounts for most

Table 2. Principal component analysis (PCA) of the five cranidial dimensions

	PC1	PC2	PC3	PC4	PC5
Eigenvalue	4.71426	0.177415	0.0837229	0.0188461	0.0057
% variance	94.285	3.5483	1.6745	0.37692	0.11491
Lg	0.99	0.0273	− 0.07412	− 0.1166	0.002215
Lab	0.9341	0.3411	0.1021	0.0255	− 0.001295
Lpl	0.9734	− 0.005985	− 0.22	0.06446	0.001492
Wp	0.9775	− 0.1739	0.1062	0.01691	0.05234
Wa	0.9791	− 0.1734	0.09017	0.01261	− 0.05474

of the variation within the sample. However, the proportion of variation is significantly lower in the remaining axes. The absolute eigenweights of Lab are lower than the rest of the longitudinal variables in the first PCA (Table 2) but higher in the second one (Table 3). In contrast, widths show lower scores in the second PCA (Table 3). This fact reflects allometric pattern growths in Lab seen in RMA. Lab, Wc and Faw also show high eigenweights in axis 2. This suggests that the second principal component is strongly associated with variation in these characters and could reflect a slight size-unrelated variability for Lab. The principal components two to five are not correlated with size. Because each principal component has influence on one or more of the variables, after removal of size, variation patterns may be seen. The bivariate plots of the three principal components display the relationships among individuals (Fig. 6a, b, d–f). The spatial distribution shows that all the specimens (including the types of all the involved species) occupy the same morphospace: the nine populations (five species) share the same morphospace, and PCA shows a single morphological group. The scores in the first component show differences in size: higher score values correspond with larger specimens. It is noteworthy that the larger specimens are the holotype and one paratype of *A. levisettii*, which are far from the main cluster but within the variation expected for larger specimens. The higher scores in the second component correspond with larger anterior borders, whereas the lower scores in this component correspond with Wp and Wa. Lpl shows higher scores in the third PCA. Thus, these characters appear to contain much of the variation of the anterior border and length of the palpebral lobe accommodated on the second and third axes, which explains the variability of these size-independent characters. PC2 shows a contrast between length and width variables, suggesting tectonic deformation of the analysed sample (in fact, these specimens come from different Moroccan and Spanish localities). PCAs from separate localities show (i) the same values for lengths and widths in axis 2 for all the Moroccan material, whereas (ii) these values are covarying in the specimens from the Spanish-type section. This fact suggests higher shape-control patterns in the Spanish material due to deformation. The discriminant function analysis of the five cranidial dimensions shows a single morphospecies within the CV (Fig. 6c)

Table 3. Principal component analysis (PCA) of the seven cranidial dimensions

	PC1	PC2	PC3	PC4	PC5	PC6	PC7
Eigenvalue	6.223	0.404187	0.177853	0.0950942	0.754691	0.01854691	0.00553074
% variance	88.905	5.7741	2.5408	1.3585	1.0781	0.26491	0.079011
Lg	0.9204	−0.1682	0.3372	0.07374	0.06892	0.02522	0.001095
Lab	0.9823	−0.1223	0.02804	−0.0542	−0.05266	−0.1168	−0.001899
Lpl	0.9657	−0.116	−0.003632	−0.1393	−0.1752	0.06178	−0.001453
Wp	0.9651	−0.1571	−0.1773	0.05787	0.07812	0.01622	−0.05164
Wa	0.9665	−0.1577	−0.1755	0.03114	0.07859	0.01297	0.05332
Faw	0.8891	0.4121	0.02715	−0.1595	0.1162	0.004865	−0.002348
Wc	0.9069	0.358	−0.01955	0.1938	−0.1072	−0.0007762	0.002927

Table 4. Pairwise comparisons of the five cranidial dimensions in the *Acaparadoxides* species showing Hotelling's *p*-values, uncorrected significance and Bonferroni corrected

	Assemame	*A. pampalius*	*A. levisettii*	*A. cf. mureroensis*	*A. ovatopyge*	*A. mureroensis*
Assemame		0.837354	0.976712	0.809112	0.812192	0.849275
A. pampalius	1		0.896899	0.964112	0.780778	5.67E-01
A. levisettii	1	1		0.835016	0.687086	7.66E-01
A. cf. mureroensis	1	1	1		0.869671	0.731221
A. ovatopyge	1	1	1	1		0.403201
A. mureroensis	1	1	1	1	1	

Table 5. Pairwise comparisons of the seven cranidial dimensions in the *Acaparadoxides* species showing Hotelling's *p*-values, uncorrected significance and Bonferroni corrected

	Assemame	*A. pampalius*	*A. levisettii*	*A. cf. mureroensis*	*A. ovatopyge*	*A. mureroensis*
Assemame		0.82703	0.892734	0.6023	0.825927	0.640756
A. pampalius	1		0.913102	0.900168	0.814324	0.352991
A. levisettii	1	1		0.663347	0.723271	0.518837
A. cf. mureroensis	1	1	1		0.61567	0.48094
A. ovatopyge	1	1	1	1		0.276016
A. mureroensis	1	1	1	1	1	

(eigenvalue = 0.2871; Wilk's lambda = 0.6487; $p < 0.5197$; Pillai trace = 0.3979; $p < 0.5102$). The discriminant function analysis of the seven cranidial dimensions shows a single morphospecies within the CV (Fig. 6f) (eigenvalue = 0.223; Wilk's lambda = 0.6476; $p = 0.896$; Pillai trace = 0.4053; $p < 0.8814$). Tables 4 and 5 document the pairwise comparison between five species (*A. nobilis* is removed because more than one specimen is needed for this analysis, whereas the holotype and topotypes of *A. mureroensis* are included). CVA provides no evidence to consider that the six species analysed here represent more than one morphotype: there is a wide overlap among all specimens in the sample. PCA and CVA results are therefore consistent with the outcome obtained by bivariate analyses.

(3) Geometric morphometrics. Figure 7 shows results from PCA of the cranidia from the Assemame paradoxidid assemblage, five *Acadoparadoxides* species described in Morocco and *A. mureroensis* from Spain. PC1 accounts for 37.9 % of the total variation and relates primarily to the glabellar length, the palpebral area width (between landmarks 7 and 13), the palpebral area width (between landmarks 2 and 10), and the position of the anterior branch of the facial suture (landmark 2) relative to the rest of the cran-

idium (Fig. 7b). PC2 accounts for 30.5 % of the total variation and is primarily related to the palpebral area width (between δ after Whittington *et al.* 1997, fig. 3, or landmark 7, and the axial furrow) and the palpebral lobe position relative to the rest of the cranidium (Fig. 7d). A smaller proportion of variation between the specimens is due to differences in the orientation of the anterior branch of the facial suture and the palpebral lobe shape (PC3, 6.5 % of total variation). The glabellar shape is rather uniform between the species, with the exception of minor differences in the proportions of the glabellar length and width. The length of the anterior border (landmarks 1 and 9) is uniform. A single canonical variate is a statistically significant discriminator of samples (Bartlett's test: Wilk's lambda = 0.0124, $\chi^2 = 226.0046$, df = 180, $p = 0.01341$, Fig. 8). Despite the substantial overlapping among the samples given in PCA, the mean morphologies of a few samples remain significantly different from one another after the Bonferroni correction (bootstrapped F-test; Table 6). There is a subtle difference between means of *A. cf. mureroensis* and *A. ovatopyge*, and between those of *A. levisettii* and *A. mureroensis*, but a high overlap among these samples in PC1/PC2 and smaller overlap in morphospace in PC2/PC3 (Fig. 7a, c). The mean morphology of *A.*
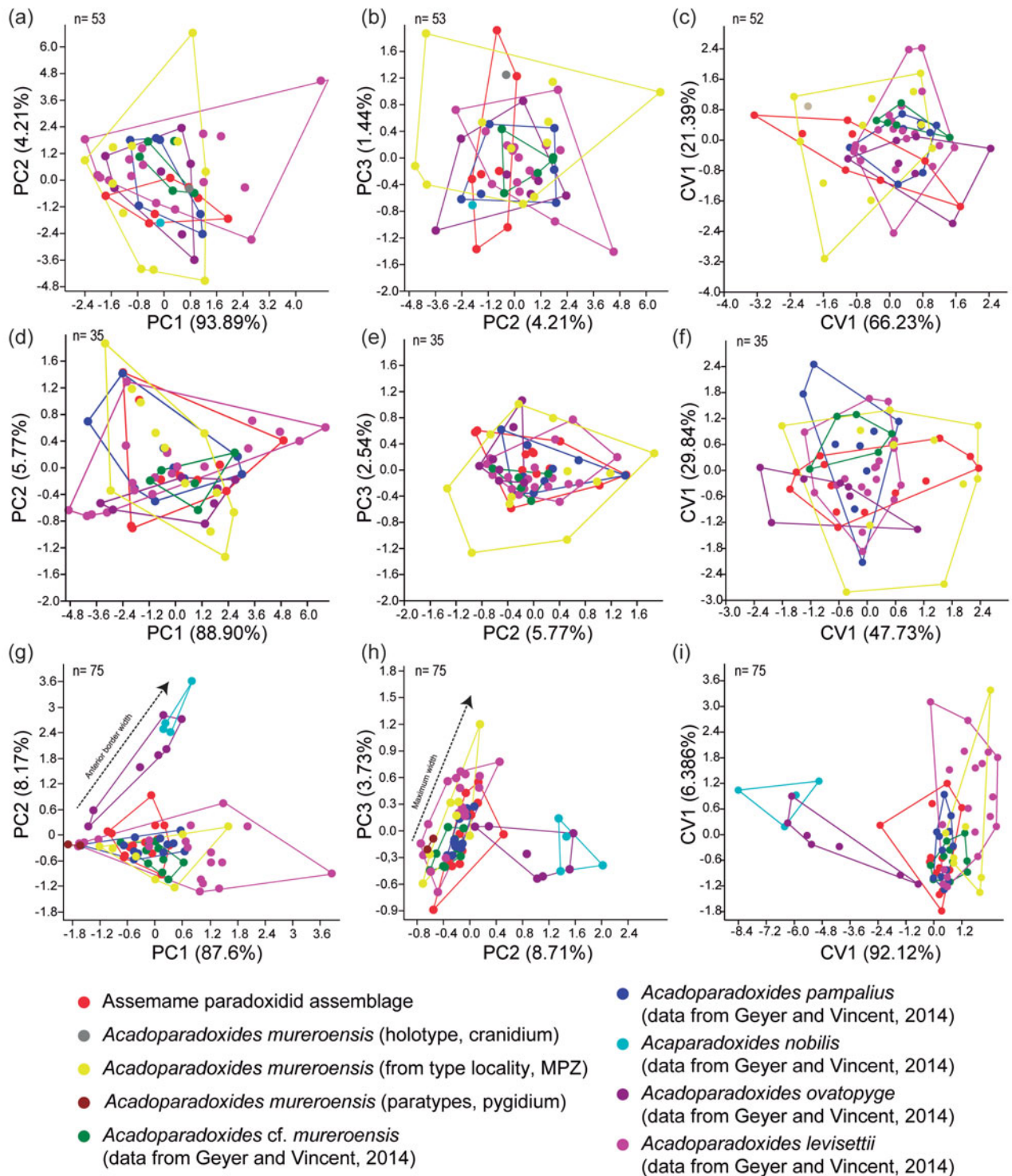
Figure 6. (Colour online) (a, b) Morphospace defined by the first three principal components of PCA related to five glabellar dimensions (see Table 2). (c) Morphospace defined by the first two axes of CVA related to five glabellar dimensions (see Table 2). (d, e) Morphospace defined by the first three principal components of PCA related to seven glabellar dimensions (see Table 3). (f) Morphospace defined by the first two axes of CVA related to seven glabellar dimensions (see Table 3). (g, h) Morphospace defined by the first three principal components of PCA related to four pygidial dimensions (see Table 8). (i) Morphospace defined by the first two axes of CVA related to four pygidial dimensions (see Table 8).

mureroensis is well represented by the holotype, which falls in the central part of the Assemame paradoxidid assemblage morphospace. By contrast, the morphological features characterizing the specimens that lie on the outer edges of the occupied morphospace include

those with either very wide or very narrow interocular areas, which mostly correspond to *A. mureroensis* from Spain.

In summary, no remarkable differences are quantified among the analysed cranidia of *A. levisettii*, *A.*
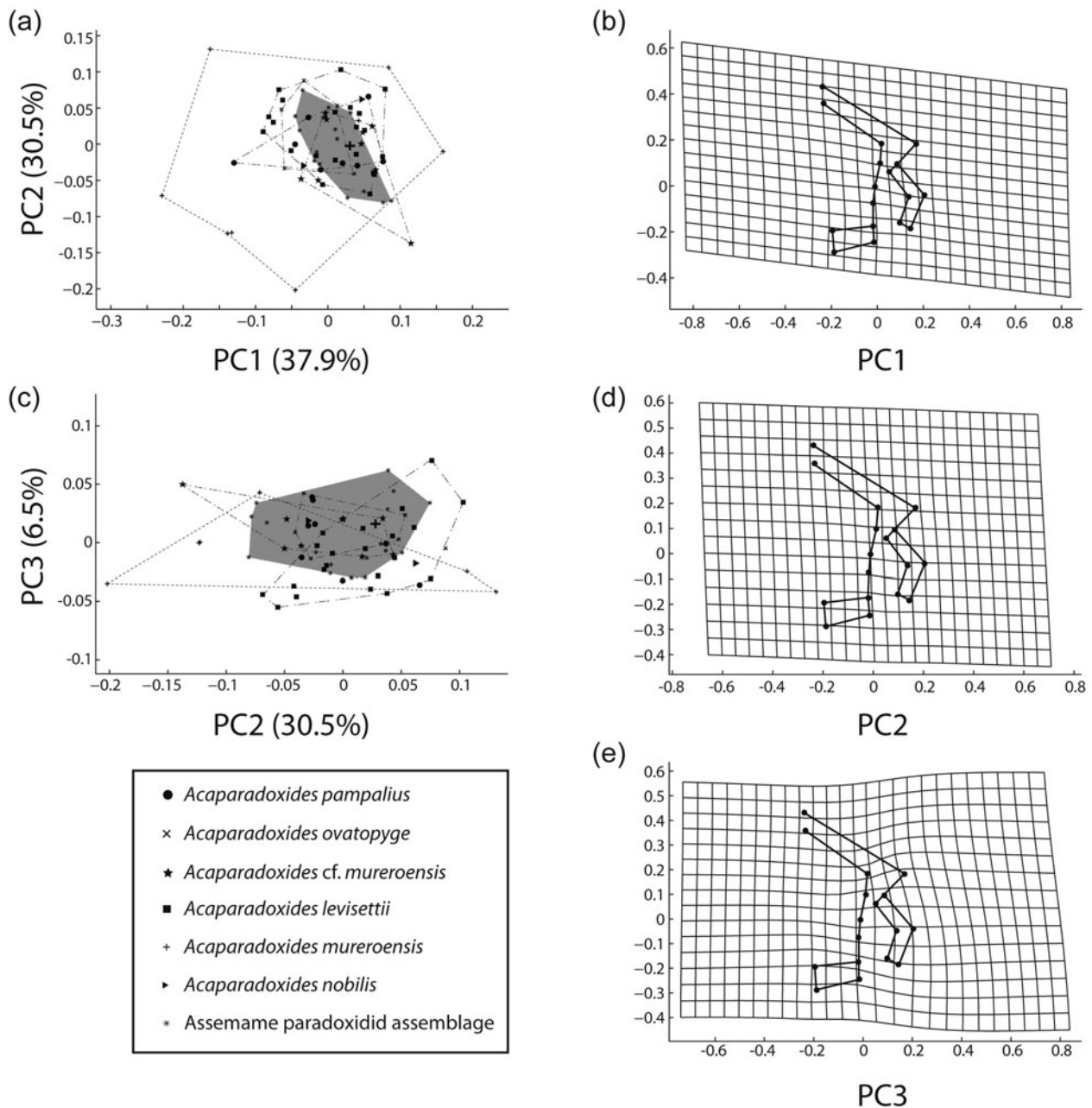
Figure 7. (a, c) Principal component analysis (PCA) of mature *Acadoparadoxides* cranidia; per cent variation summarized by each axis shown in axis label; shaded area represents the Assemame paradoxid assemblage morphospace, and large cross the holotype of *Acadoparadoxides mureroensis*. (b, d, e) Thin-plate spline projections of variation along (b) PC1, (d) PC2, (e) PC3 (see Fig. 4a for landmark configuration).

mureroensis, *A.* cf. *mureroensis*, *A. nobilis*, *A. ovato-pyge* and *A. pampalius*.

5.b. Pygidia

As explained above, the pygidial morphology is key to distinguish species in *Acadoparadoxides*. For the bivariate (RMA) and multivariate (PCA) analyses, four linear variables have been assessed: two axial (Al and Sl) and two transverse (Aw and Mw). The four variables characterize the overall shape of the pygidium and have been used to define several species of *Acadoparadoxides*. In addition, the geometric morphomet-

ric method allows the inclusion of 11 landmarks to improve the overall shape quantification of the pygidium. The posterior width of the pygidia has not been used due to the difficulty of taking accurate measurements.

(1) Bivariate analysis (RMA). The morphological variation of each pygidial character has been assessed with respect to a standard measure for pygidial size. The latter has been chosen as Sl due to axial features being relatively constant in trilobites (see Palmer, 1957; Hughes, 1994).

Al. RMA shows that the growth of Al is isometric with respect to Sl at the 95 % confidence level ($n = 78$, $a = 0.993$, $b = -0.108$, $r = 0.99$, $p < 0.0001$, Fig. 9a).
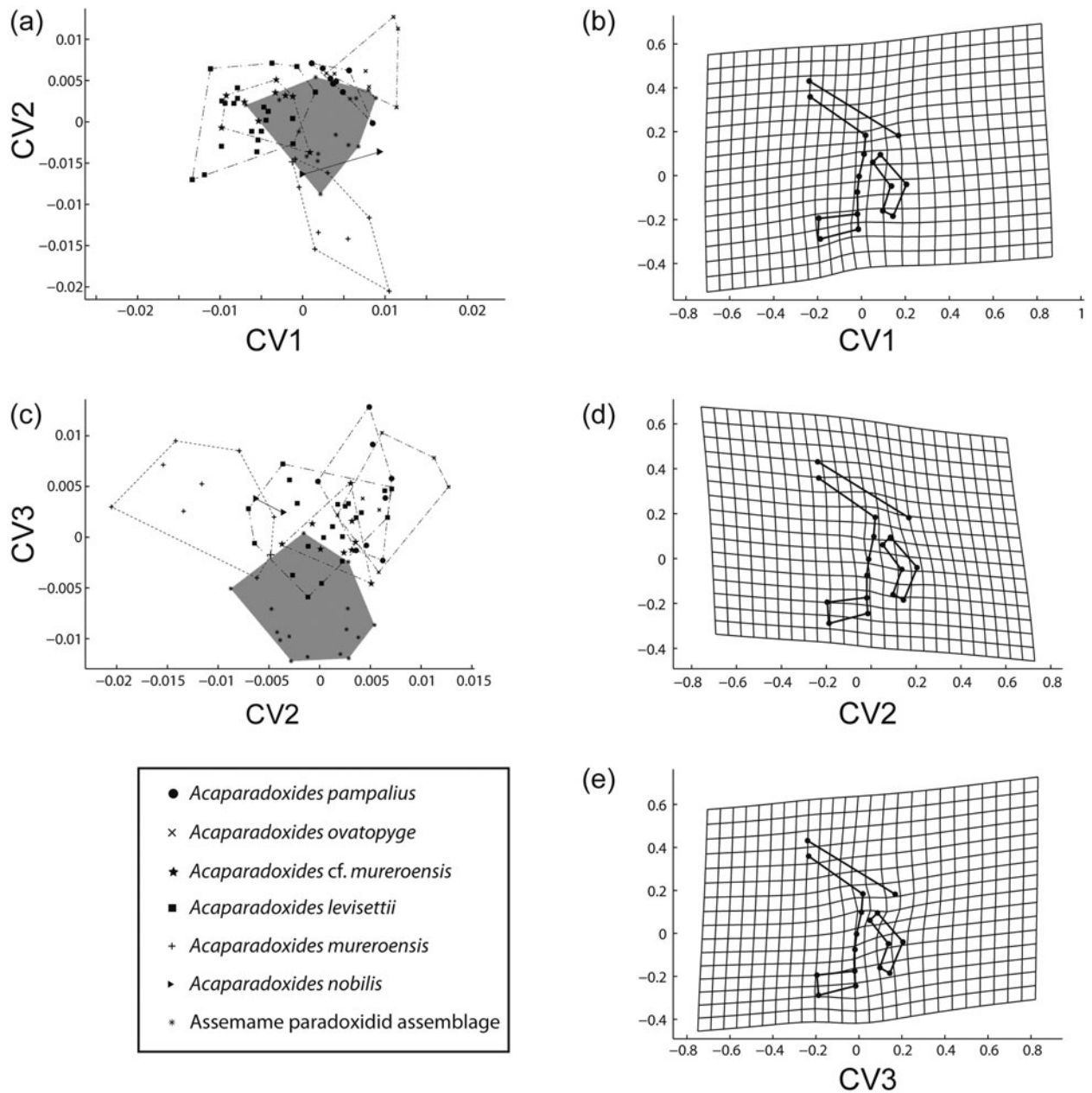
Figure 8. (a, c) Canonical variates analysis (CVA) of mature *Acadoparadoxides* cranidia; shaded area represents the Assemame para-doxidid assemblage morphospace, and the large cross the holotype of *Acadoparadoxides mureroensis*. (b, d, e) Thin-plate spline projections of variation along (b) CV1, (d) CV2, (e) CV3 (see Fig. 4a for landmark configuration).

Within the sample, the growth of Al shows small variations.

Aw. RMA shows that the growth of Aw is isometric with respect to Sl at the 95 % confidence level ($n = 78$, $a = 1.059$, $b = -0.22$, $r = 0.95$, $p < 0.0001$, Fig. 9b). Within the sample, the growth of Aw shows a considerable variation among the larger specimens (between 9 and 18 mm sagittal length). The bivariate plot shows interpopulational differences, which are observable in the slightly different trends of the regression lines for each population. The populations of *A. nobilis* and *A. ovatopyge* seem to have a wider anterior border and show a sloping regression line, so larger specimens of these species have a relatively wider anterior border by comparison with our sample.

Mw. RMA shows that the growth of Mw is isometric with respect to Lg at the 95 % confidence level ($n = 78$, $a = 1.027$, $b = -0.05$, $r = 0.95$ $p < 0.0001$, Fig. 9c). Comparison between the regression coefficients of these variables was carried out based on a MANOVA (Wilk's lambda: 0.07988, df1: 3, df2: 71, F: 735.5, $p < 0.00001$). RMA suggests that all species represent a single morphospecies. However, it is possible (if viewed synoptically) that multiple measurements could reveal the presence of separate clusters.

(2) Multivariate analysis (PCA). The correlation matrix of 75 specimens of *Acadoparadoxides mureroensis*, *A.* cf. *mureroensis*, *A. levisettii*, *A. nobilis*, *A. ovatopyge* and *A. pampalius* shows relatively low values between the anterior width and the sagittal length,
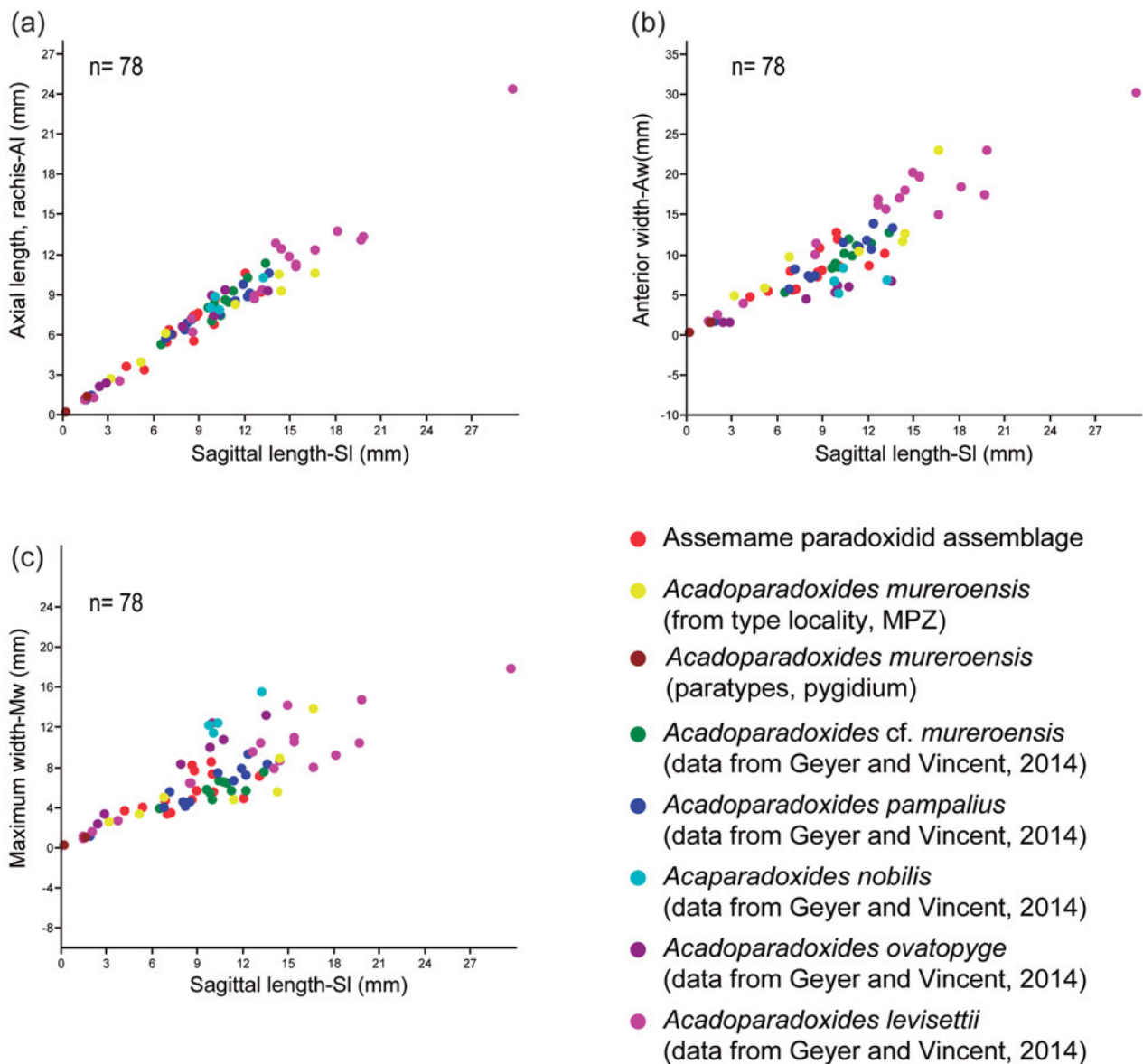
Figure 9. (Colour online) Bivariate plots showing the relationship between the sagittal length and the axial length of the rachis (a), the anterior width (b) and the maximum pygidial width (c).

and between both the width and length of the axis, suggesting highly independent size variability in these characters.

The eigenvalues show how much of the variation is accounted for by each principal component, and the PC loadings of each variable to each principal component have also been calculated as the eigenweights (Table 4). The first and second components account for most of the variation within the sample in the analysis (PC1: 87.6 %, PC2: 8.17 %, PC3: 3.73 %; Fig. 6g, h). All variables (on PC1) have positive PC loadings and are roughly similar among all variables, with the exception of Aw (Table 7). These results suggest that the first component is related to the overall size of the specimens, and this accounts for most of the variation within the sample. However, the low eigenweight of the anterior width and the low values of correlation with Sl confirm its size-independent variability. Fur-

thermore, the load of the anterior width in the second axis has a very high value, supporting the idea that the variation of this variable is not related to size. This variability may be associated with intraspecific variation, but its occurrence in axis 2 suggests that these specimens may belong to different taxa. Figure 6g, h shows the bivariate plot of the first three principal components. There, *A. nobilis* and *A. ovatopyge* display different trends: the higher scores of component 2 correspond with wider anterior borders. This different trend suggests that these two species are, in fact, different from the rest of the analysed species and they may likely be conspecific. After removing both taxa from PCA, the first and second components account for 98 % of the variation within the sample (PC1: 94.866 %, PC2: 3.953 %). In the second PCA, all variables have positive PC loadings and are similar, showing slightly higher scores for the first axis in Aw and

Table 6. Pairwise comparison of *Accadoparadoxides* species from Spain and Morocco based on dataset from cranidial shape. *F*- and *P*-value based on 1600 bootstraps. *P*-value significant at $\alpha = 0.05$ in all cases in bold; *P*-value significant at $\alpha = 0.05$, after Bonferroni correction, in italics; and *P*-value significant at $\alpha = 0.05$, but not after Bonferroni correction, underlined

	F	P-value	F	P-value
Assemame vs *A.* cf. *mureroensis*	1.02	0.44296	1.02	0.3562
Assemame vs *A. levissettii*	1.08	0.35584	1.08	0.35
Assemame vs *A. mureroensis*	1.91	**0.00274**	1.91	0.1375
Assemame vs *A. nobilis*	0.38	0.99	0.38	0.8744
Assemame vs *A. ovatopyge*	1.26	0.1646	1.26	0.2706
Assemame vs *A. pampalius*	0.51	0.986	0.51	0.7506
A. cf. *mureroensis* vs *A. levisettii*	1.61	**0.0204**	1.61	0.1388
A. cf. *mureroensis* vs *A. mureroensis*	1.93	**0.026**	1.93	0.1425
A. cf. *mureroensis* vs *A. nobilis*	0.69	0.88625	0.69	0.57
A. cf. *mureroensis* vs *A. ovatopyge*	2.53	**<0.0001**	2.53	0.0706
A. cf. *mureroensis* vs *A. pampalius*	1.01	0.449	1.01	0.4019
A. levisettii vs *A. mureroensis*	2.2	**0.0002**	2.2	0.08
A. levisettii vs *A. nobilis*	0.23	1	0.23	0.97
A. levisettii vs *A. ovatopyge*	0.94	0.566	0.94	0.4319
A. levisettii vs *A. pampalius*	0.70	0.8877	0.70	0.613
A. mureroensis vs *A. nobilis*	0.37	0.99	0.37	0.75
A. mureroensis vs *A. ovatopyge*	0.81	0.757	0.81	0.45
A. mureroensis vs *A. pampalius*	0.79	0.786	0.79	0.4869
A. nobilis vs *A. ovatopyge*	0.45	0.994	0.45	0.788
A. nobilis vs *A. pampalius*	0.39	0.9984	0.39	0.8438
A. ovatopyge vs *A. pampalius*	0.73	0.855	0.73	0.565

Table 7. Principal component analysis (PCA) of the four pygidial dimensions

	PC1	PC2	PC3	PC4
Eigenvalue	3.50415	0.326845	0.149349	0.0196539
% variance	87.604	8.1711	3.7337	0.49135
Sl	0.9841	− 0.07909	− 0.1149	− 0.11
Al	0.9657	− 0.08708	− 0.2298	0.08377
Aw	0.8697	0.4837	0.09776	0.009292
Mw	0.9202	− 0.2812	0.2716	0.02099

Table 8. Principal component analysis of the four pygidial dimensions without *A. nobilis* and *A. ovatopyge*

	PC1	PC2	PC3	PC4
Eigenvalue	80.67	3.362	0.63977	0.363808
% variance	94.866	3.9538	0.75235	0.42783
Sl	0.9807	0.1757	0.03511	− 0.07758
Al	0.9564	0.2678	− 0.02637	0.1134
Aw	0.9547	− 0.2277	0.186	0.04647
Mw	0.9829	− 0.1674	− 0.07691	− 0.00478

Mw (Table 8). However, Aw and Mw exhibit negative values in the second axis. These characters show an antagonistic behaviour for Sl and Al. PC3 also shows an antagonistic behaviour of Sl and Mw: specimens with larger sagittal lengths display narrower Mw values, and vice versa. Aw also shows a high loading in PC3. Thus, these characters appear to contain much of the variation of the anterior border, sagittal length and maximum widths accommodated on the second and third axes, which explains the variability in these size-independent characters. The results in the first PCA show the same sign for lengths and widths in axis 2, except for Aw for the whole sample (Table 7) and a positive sign in the second PCA (Table 8). PCAs of

separate samples show similar values, which suggest some variation controlled by tectonic deformation.

A discriminant function analysis of the four pygidial dimensions shows that the two species recognized within PCA (*A. nobilis* and *A. ovatopyge*) are significantly different from the rest of the species (eigenvalue = 4.274; Wilk's lambda = 0.1344; $p < 0.0001$, Fig. 6i). In addition, *A. levisettii* seems to be significantly different from the Assemame assemblage. Hotelling's *p*-values, uncorrected significance and Bonferroni corrected confirm this result (Table 9). These suggest that the pygidial differences, such as shape (subovate, subelongate, sub-rounded and subhexagonal), well-defined platform of the rachis (short rachis with well-defined platform, large rachis with poorly defined platform) or rachis length have a high size-unrelated variability. PCA demonstrates a continuous variation between the analysed species, so that morphotypes cannot be discriminated.

Although *A. nobilis* and *A. ovatopyge* might be *a priori* conspecific, a geometric morphometric analysis seems necessary to better quantify their small differences, not yet evaluated. Similar patterns were documented in the pygidia of *Paradoxides davidis* by Bergström & Levi-Setti (1978), *P. paradoxissimus* by Weidner & Nielsen (2009), *Eccaparadoxides pradoanus* by Esteve (2014), and unnamed paradoxidid sclerites from Scandinavia by Weidner & Nielsen (2014). These studies point out the high variation of the paradoxidid pygidia, which makes for difficult taxonomic assignation based on few specimens.

(3) Geometric morphometrics. Figure 10 shows results from PCA of the pygidia from the Assemame paradoxidid assemblage, five species from Morocco and one from Spain. PC1 accounts for 38.1 % of the total variation and relates primarily to the position and width of the maximum width (landmark 4) to the rest of the pygidium (Fig. 10b). PC2 accounts for 28.6 % of the total variation and is primarily related to the position of the maximum width, length of the axial ring and pygidial anterior border width (landmarks 1–3) to the rest of the pygidium (Fig. 10d). A very small proportion of the variation between specimens is controlled by the platform position (landmark 7), the relative width of the posterior border (landmarks 5 and 6) and the small variation in the position of the maximum anterior width (landmark 4) (PC3, 0.13 % of total variation; Fig. 10e). Unlike the cranidia, the morphological means of more species remain significantly different from one another after Bonferroni correction (bootstrapped F-test; Table 10). For instance, *A. ovatopyge* and *A. pampalius* differ significantly from *A.* cf. *mureroensis* after Bonferroni correction (bootstrapped F-test). Thus, there is more morphological separation along PC1 in the pygidia than in the cranidia. In fact, all pygidia overlap except *A. nobilis*. The latter is separated from the rest of the *Acadopadoxides* species by PC1 and small overlap in PC3 (Fig. 10a, c). Two canonical variates are statistically significant discriminators of samples (Bartlett's

Table 9. Pairwise comparisons of the four pygidial dimensions in the *Acaparadoxides* species showing Hotelling's *p*-values, uncorrected significance and Bonferroni corrected, *p*-value significant at $\alpha = 0.05$ in bold.

|	Assemame	A. cf. *mureroensis*	A. *pampalius*	A. *levisettii*	A. *mureroensis*	A. *nobilis*	A. *ovatopyge*
Assemame		0.519238	0.971877	**9.85E-04**	0.1132	**2.53E-06**	**7.28E-06**
A. cf. *mureroensis*	1		0.726141	**1.21E-03**	0.253031	**4.00E-05**	**2.91E-05**
A. *pampalius*	1	1		**5.37E-04**	0.257985	**3.70E-06**	**6.30E-06**
A. *levisettii*	**2.07E-03**	0.255636	0.112934		0.304743	**1.95E-09**	**1.45E-09**
A. *mureroensis*	1	1	1	1		**5.77E-04**	**1.41E-03**
A. *nobilis*	**5.31E-05**	**8.40E-04**	**7.77E-05**	**4.09E-08**	**1.21E-02**		0.13897
A. *ovatopyge*	**1.52E-05**	**6.11E-0.457**	**1.32E-0.4**	**3.05E-08**	**2.96-E03**	1	
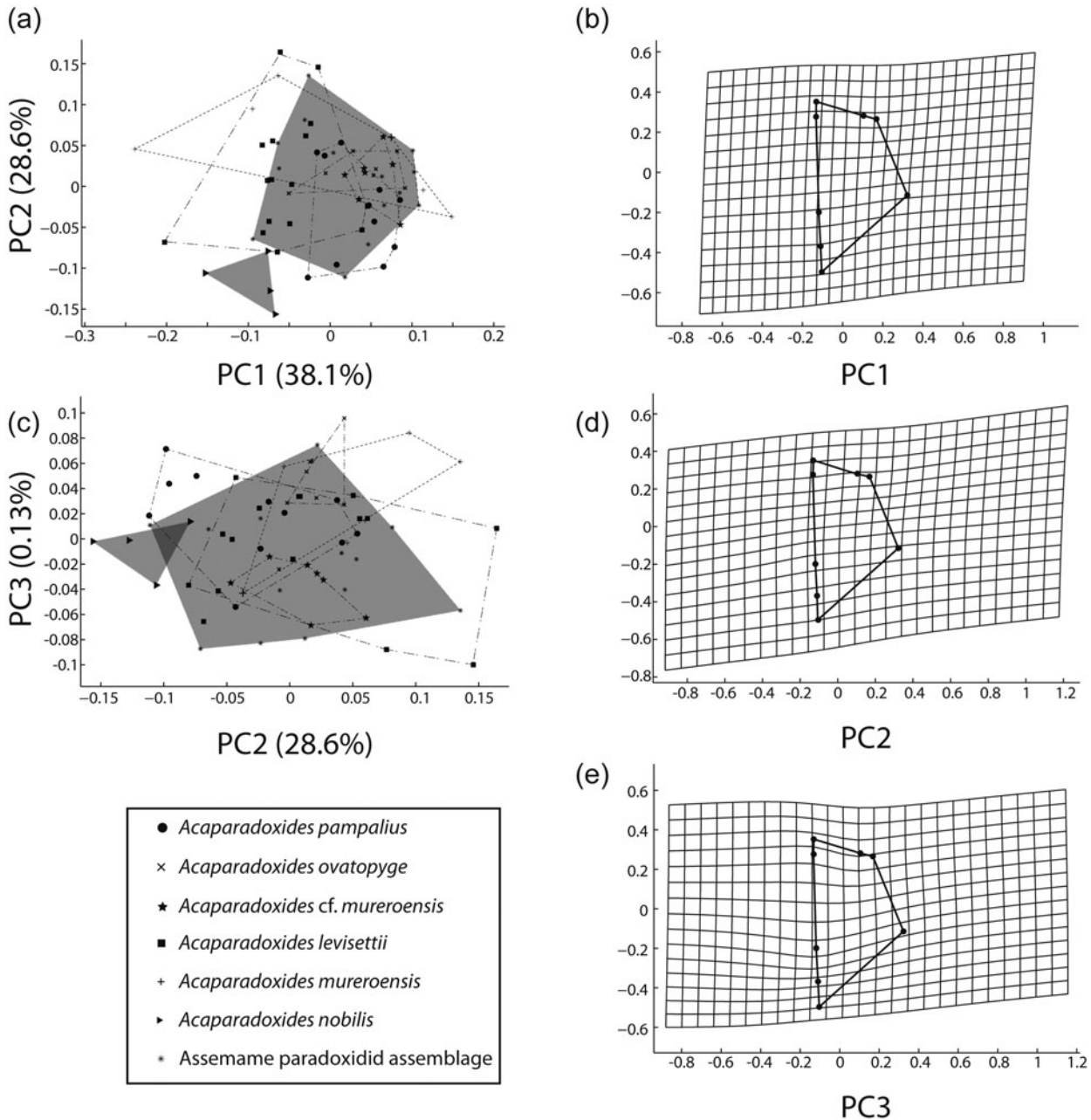
Figure 10. (a, c) Principal component analysis (PCA) of pygidial landmark data in *Acadoparadoxides* species. Per cent variation summarized by each axis shown in axis label. Shaded area represents Assemame paradoxid assemblage morphospace, large cross represents *Acadoparadoxides mureroensis* topotype (MPZ2004/59). (b, d, e) Thin-plate spline projections of variation along (b) PC1, (d) PC2, (e) PC3 (see Fig. 4 for landmark configuration).

Table 10. Pairwise comparison of *Accadoparadoxides* species from Spain and Morocco based on dataset from pygidial shape. *F* and *P*-value based on 1600 bootstraps. *P*-value significant at α = 0.05 in all cases in bold; *P*-value significant at α = 0.05, after Bonferroni correction, in italics, and *P*-value significant at α = 0.05, but not after Bonferroni, correction underlined

	F	P-value	F	P-value
Assemame vs *A.* cf. *mureroensis*	1.09	0.37173	1.09	0.3381
Assemame vs *A. levissettii*	1.51	0.12053	1.25	0.288
Assemame vs *A. mureroensis*	1.51	0.12053	1.51	0.2269
Assemame vs **A. nobilis**	**8.13**	**<0.0001**	8.13	*0.0006*
Assemame vs *A. ovatopyge*	1.58	0.099	1.59	0.155
Assemame vs *A. pampalius*	1.96	**0.0277**	1.96	0.115
A. cf. *mureroensis* vs *A. levisettii*	2.11	**0.020104**	2.11	0.1369
A. cf. *mureroensis* vs *A. mureroensis*	2.11	**0.020104**	2.11	0.1306
A. cf. *mureroensis* vs **A. nobilis**	22.57	0	22.57	*0.0006*
A. cf. *mureroensis* vs *A. ovatopyge*	4.79	**<0.0001**	4.79	*0.0031*
A. cf. *mureroensis* vs *A. pampalius*	4.03	**<0.0001**	4.03	*0.0088*
A. levisettii vs *A. mureroensis*	2.20	0.19671	1.37	0.2712
A. levisettii vs **A. nobilis**	4.69	**<0.0001**	4.69	*0.011*
A. levisettii vs *A. ovatopyge*	4.58	**<0.0001**	4.58	*0.0038*
A. levisettii vs *A. pampalius*	4.05	**0.015007**	6.57	*0.0006*
A. mureroensis vs **A. nobilis**	4.06	**<0.0001**	4.06	*0.0319*
A. mureroensis vs *A. ovatopyge*	0.77	0.68	0.77	0.484
A. mureroensis vs *A. pampalius*	2.44	**0.0057**	2.44	*0.068*
A. nobilis vs *A. ovatopyge*	14.27	0	14.27	*0.0006*
A. nobilis vs *A. pampalius*	9.67	**<0.0001**	9.67	*0.006*
A. ovatopyge vs *A. pampalius*	1.95	**0.03102**	1.95	0.1038

Table 11. Percentage of total variance (SStotal, measured as summed squared Procrustes units) explained by allometry in the samples of all analysed species. *P*-value is based on 1600 bootstraps

Species / Assemblage	SS_{total}	$SS_{residual}$	% variance explained	P
Assemame	0.1384	0.1104	20.2413	0.043750
A. levisettii	0.13001	0.1254	3.6679	0.71
A. cf. *mureroensis*	0.0303	0.0262	13.2614	0.57
A. mureroensis	0.0862	0.0513	40.5288	0.105
A. nobilis	0.0191	0.0136	28.8461	0.368
A. ovatopyge	0.0419	0.0322	23.3210	0.211250
A. pampalius	0.0628	0.0515	17.9841	0.1412

test: Wilk's lambda = 0.0462, χ^2 = 167.5450, df = 72, $p < 0.00001$; Wilk's lambda = 0.1656, χ^2 = 98.002, df = 55, $p < 0.00032302$, Fig. 11).

A second analysis was performed after removing *A. nobilis*. PC1 accounts for 40.4 % and relates to the maximum width (landmark 4), and length of the posterior border (landmarks 5 and 6) to the rest of the pygidial shape. PC2 accounts for 24.5 % of the total variation, and relates to the general position of the maximum width (landmark 4) to the rest of the pygidium. PC3 accounts for 14.8 % of the total variation, and relates to the relative position of the platform with respect to the axial ring (landmarks 7 and 8). In this case, three canonical variates are statistically significant discriminators of samples (Bartlett's test: Wilk's lambda = 0.0740, χ^2 = 132.7835, df = 60, $p < 0.00001$; Wilk's lambda = 0.1870, χ^2 = 85.7747, df = 44, p < 0.000166271; Wilk's lambda = 0.4174, χ^2 = 44.5554, df = 30, $p < 0.0424368$).

In order to assess the pygidial and rachis outlines, the above results were evaluated using a second approach through semi-landmarks. Figure 12 shows PCA results of the pygidia from Assemame, five species from Morocco and one from Spain. PC1 accounts for 50.53 % of the total variation and relates primarily to the position and ratio of maximum pygidial width (landmark 4) (Fig. 12a). The relative width ranges from narrower pygidia with wider rachis (Fig. 12a1) to wider pygidia with narrower rachis (Fig. 12a2). PC2 accounts for 10.08 % of the total variation and, as in the case of the landmarks approach, it is primarily related to the relative position of the maximum width, the length of axial ring and the pygidial anterior border width (landmarks 1–3) (Fig. 12a), as well as the

relative length and width of the rachis. Thus, the pygidia with larger (sag.) axial rings have longer (sag.) and narrower (tr.) rachis (Fig. 12a3), and the pygidia with shorter (sag.) axial rings have shorter (sag.) and wider (tr.) rachis (Fig. 12a4). PC3 (Fig. 12b) accounts for 10.3 % of the total variation between specimens: it is controlled by the platform position (landmark 7), the relative width (tr.) of the posterior border (landmarks 5 and 6), and the small variation in the position of the maximum anterior width (landmark 4). However, the rachis displays more variation, ranging from very wide (tr.) and relatively long (sag.) rachis with narrower (sag.) posterior border (Fig. 12b5) to very narrow (tr.) and relatively narrow (sag.) rachis with wider (sag.) posterior border (Fig. 12b6).

The proportion of total shape variance explained by allometry was calculated for each species using Regress8 software (Sheets, 2014). The mean pygidial shape of each population/species was calculated as the consensus of all configurations of that species (Fig. 13). The total shape variance (SStotal) of that species was quantified as the summed squared partial Procrustes distances of all configurations of that species to its mean shape. Partial warp scores were then calculated for each configuration away from the reference configuration of that species, and those scores were regressed in a multivariate regression against lnCS to produce a vector of regression coefficients describing the nature of shape change over the sampled portion of ontogeny for each species. The summed squared residuals (SSresidual) from this regression, also expressed in Procrustes units, represent shape deviations that are not attributable to allometry. The difference between SStotal and SSresidual gives the variance explained by the allometry regression (SSmodel), and the ratio of SSmodel to SStotal gives the proportion of total variance explained by allometry. Nonparametric resampling (1600 bootstraps) determines the statistical significance of the multivariate regression. Using this method, allometry explains 20.2 % of the total shape variation in the sample of the *Accaparadoxides* population from Assemame, only 3.66 % in *A. levisettii*, 13.26 % in *A.* cf. *mureroensis*, 40.5 % in *A. mureroensis*, 28.8 % in *A. nobilis*, 23.3 % in *A. ovatopyge*, and 17.9 % in *A. pampalius* (Table 11). The proportion of total shape variance explained by
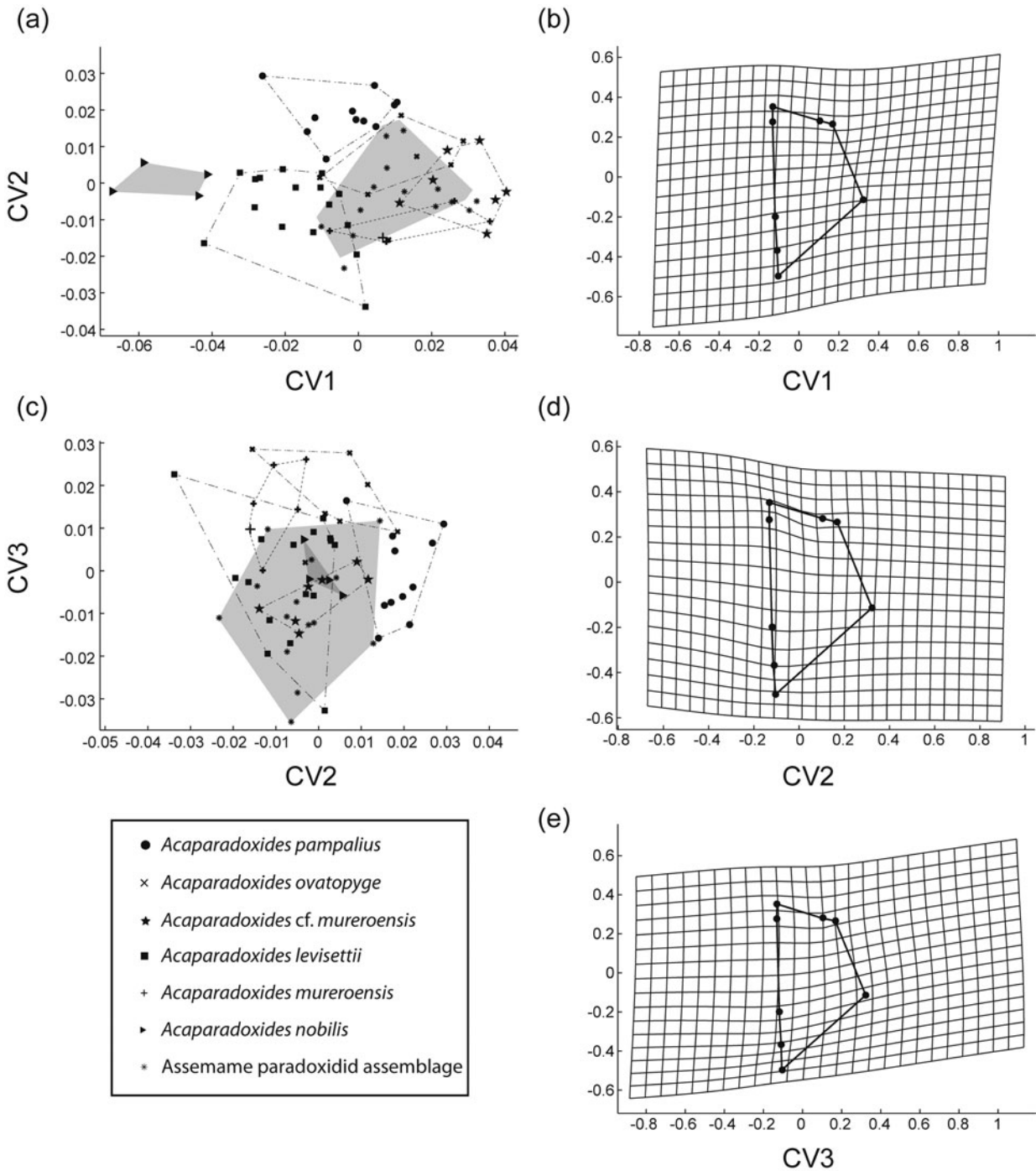
Figure 11. (a, c) Canonical variates analysis (CVA) of mature *Acadoparadoxides* pygidia; shaded area represents the Assemame paradoxid assamblage morphospace, and the large cross the topotype of *Acadoparadoxides mureroensis*. (b, d, e) Thin-plate spline projections of variation along (b) CV1, (d) CV2, (e) CV3 (see Fig. 4c for landmark configuration).

allometry in *A. levisettii* is smaller (3.66 %) but not representative ($P = 0.71$). Such a difference in strength of the allometric signal when comparing data from *A. levisettii* and the remaining species is not surprising, as the population of *A. levisettii* is biased by large pygidia, which are poorly represented in the other samples.

In order to assess the difference in the mean pygidial shape, two non-parametric tests were carried out. Parametric tests of difference in mean shape between species are inappropriate because of the incorporation of semi-landmarks in that configuration

(affecting the estimate of degrees of freedom). However, statistical tests based on bootstrap resampling, which do not require estimates of degrees of freedom, are appropriate. For each pairwise species comparison, two such non-parametric tests were performed using the TwoGroup8 software (Sheets, 2014). The first non-parametric test demonstrates that the partial Procrustes distance between the mean pygidial shape of each species is not significantly different from zero in all pairwise comparisons with size standardization (confidence limits determined by 1600 bootstraps;
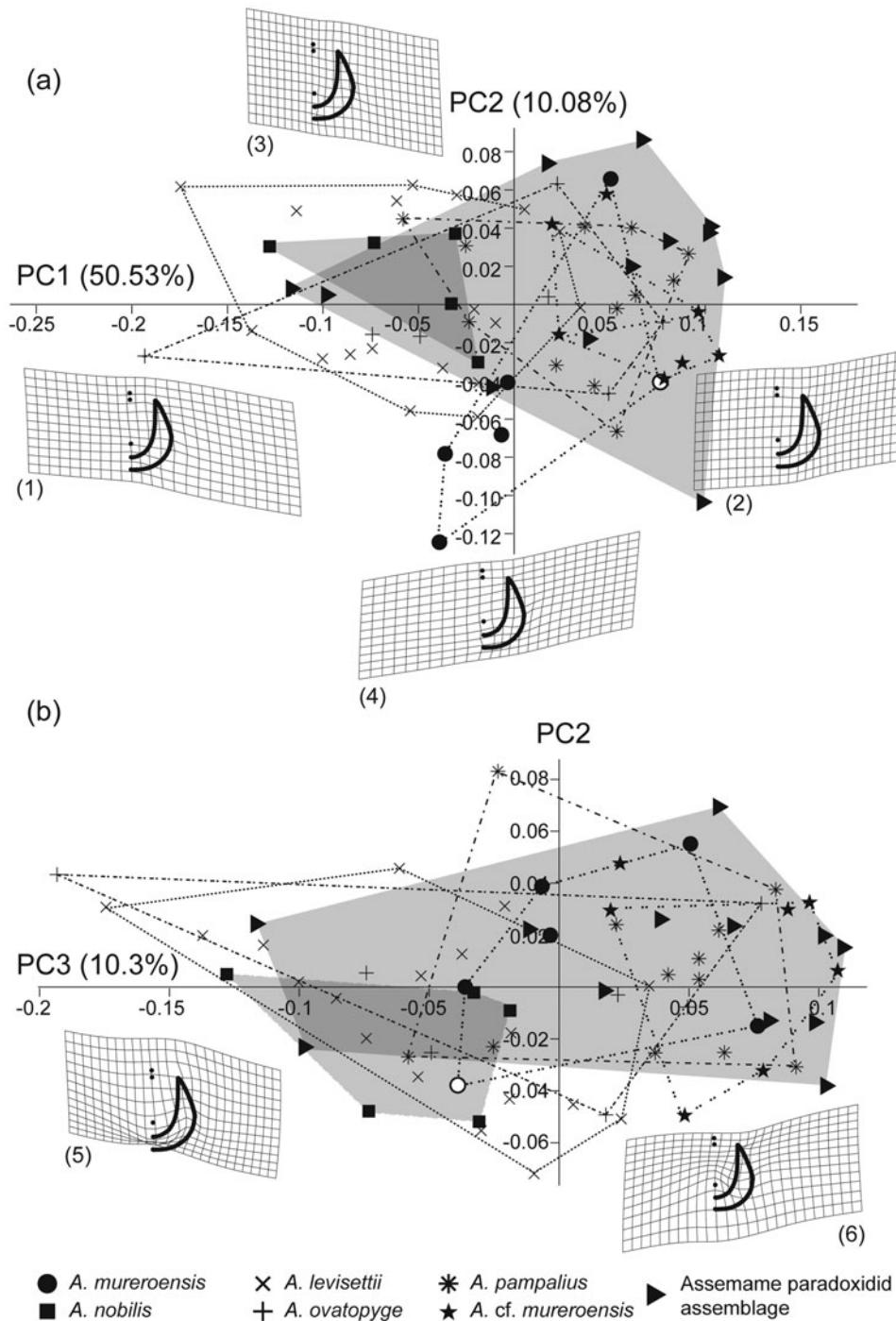
Figure 12. (a, b) Principal component analysis (PCA) of pygidial semi-landmark data in the species of *Acadoparadoxides*. Per cent variation summarized by each axis shown in axis label. (1) Thin-plate spline projection of variation in negative axis (score: −0.15) in PC1. (2) Thin-plate spline projection of variation in positive axis (score: 0.10) in PC1. (3) Thin-plate spline projection of variation in positive axis (score: 0.06) in PC2. (4) Thin-plate spline projection of variation in negative axis (score: −0.12) in PC2. (5) Thin-plate spline projection of variation in negative axis (score: −0.20) in PC3. (6) Thin-plate spline projection of variation in positive axis (score: −0.10) in PC3. Shaded area represents the Assemame paradoxidid assemblage morphospace, and the large cross the *Acadoparadoxides mureroensis* topotype (MPZ2004/59).

Table 12). The second non-parametric test investigates between-sample differences in mean shape using a bootstrap-based approach utilizing Goodall's F-test (Goodall, 1991; Dryden & Mardia, 1998) of Procrustes distance between sample means as the test statistic (see Webster & Sheets, 2010). The observed F-value is compared to the range of F-values obtained by randomly assigning specimens to samples (1600 replicates). This test yields significant differences in the mean shape between *A. levisettii*, *A. nobilis* and the remaining species (Table 12). *A. mureroensis*, *A. cf. mureroensis*, *A. pampalius*, *A. ovatopyge* and the Assemame population show no remarkable differences in the mean shape.
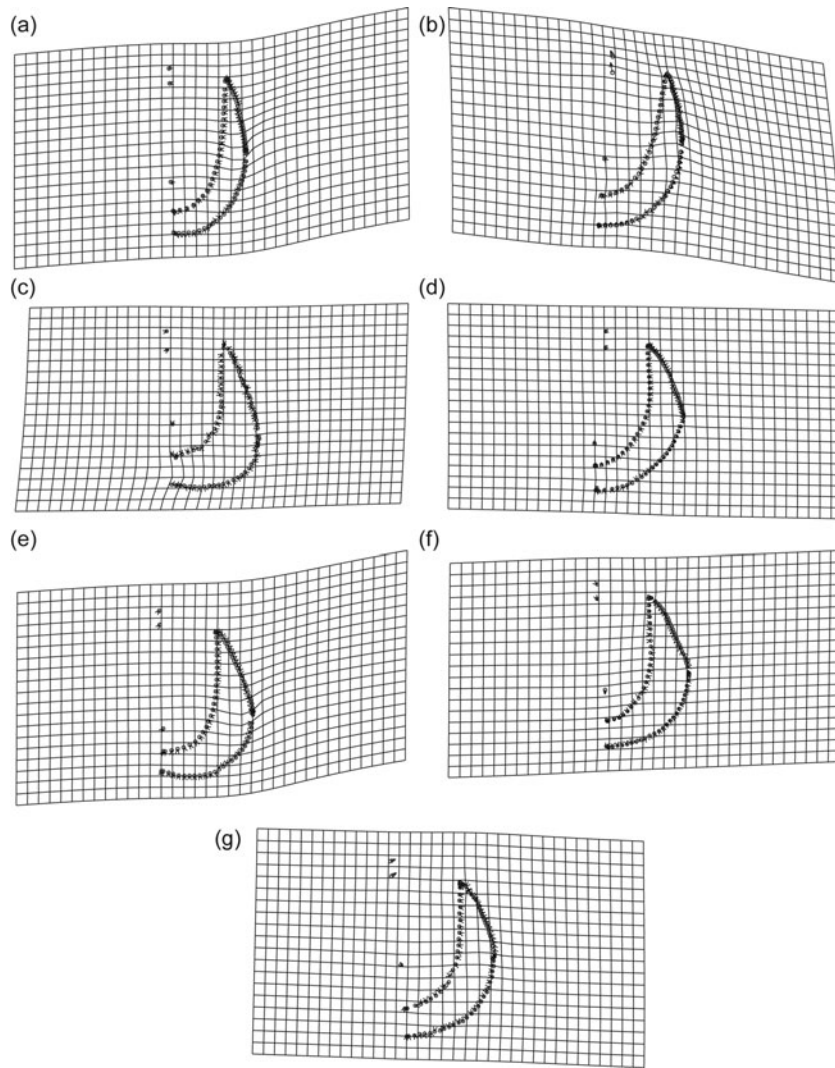
Figure 13. Thin-plate spline deformation grids depicting the intraspecific shape variation in each species of *Acadoparadoxides*. Shape variation was calculated by a regression of shape variables against lnCS for each sample; the reference forms in each plot are the three smallest specimens of each population.

Table 12. Pairwise non-parametric statistical comparisons of mean cranidial shape between all analysed species. Lower and upper 95 % confidence limits and significance value of Goodall's F-test based on 1600 bootstraps

species comparison	Partial procrustes distance			Goodall's F-test	
	between species means	lower 95% limit	upper 95% limit	F	P
Assemame to *A. levisettii*	0.1121	0.0855	0.1525	9.63	**0.0006**
Assemame to cf. *A. mureroensis*	0.0453	0.0354	0.019	1.00	0.3681
Assemame to *A. mureroensis*	0.0916	0.0660	0.1655	2.61	0.0769
Assemame to *A. nobilis*	0.1210	0.871	0.1676	5.35	**0.0088**
Assemame to *A. ovatopyge*	0.0474	0.0937	0.0139	1.02	0.3812
Assemame to *A. pampalius*	0.0259	0.0265	0.0721	0.44	**0.0118**
A. levisettii to *A.*cf. *mureroensis*	0.1521	0.1323	0.1827	15.65	**0.0006**
A. levisettii to *A. mureroensis*	0.1036	0.0960	0.1503	4.61	**0.0056**
A. levisettii to *A.nobilis*	0.0384	0.0359	0.0721	0.76	0.5337
A. levisettii to *A. ovatopyge*	0.0881	0.0614	0.1342	4.92	**0.0044**
A. levisettii to *A. pampalius*	0.1025	0.0832	0.1367	9.43	**0.0006**
A. cf. *mureroensis* to *A. mureroensis*	0.1150	0.0803	0.1852	4.03	**0.0231**
A. cf. *mureroensis* to *A. nobilis*	0.1616	0.1329	0.2020	15.32	**0.0006**
A. cf. *mureroensis* to *A. ovatopyge*	0.0782	0.0612	0.1189	3.55	**0.0206**
A. cf. *mureroensis* to *A. pampalius*	0.0561	0.0454	0.0914	2.31	0.0656
A. mureroensis to *A. nobilis*	0.1101	0.0988	0.1588	2.82	0.0631
A. mureroensis to *A. ovatopyge*	0.0804	0.0649	0.1521	1.79	0.1656
A. mureroensis to *A. pampalius*	0.0876	0.697	0.1541	2.99	**0.036**
A. nobilis to *A. ovatopyge*	0.0997	0.0717	0.1530	4.74	**0.0162**
A. ovatopyge to *A. pampalius*	0.0410	0.0369	0.0793	1.10	0.3369

(a)

(b)
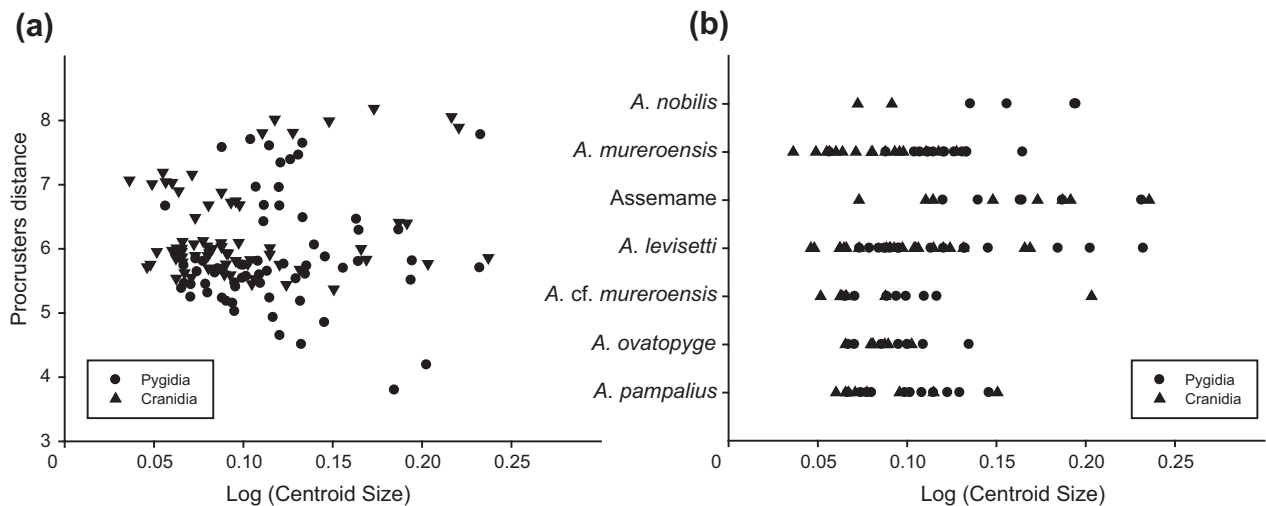

Figure 14. (a) Procrustes distance of each specimen from the mean configuration against log centoid size. (b) Range of centroid size for each species and specimens from Assemame open quarry.

5.c. Ontogenic control

To explore the overall ontogenetic trends in the above-reported paradoxidid species, we used the Procrustes distance from a reference form. Procrustes distance is the square root of the sum of squared differences between the positions of the landmarks in two optimally superimposed (by least-squares) configurations. A consensus specimen of the three smallest specimens was used as a reference specimen in calculating the Procrustes distances of all specimens (53 cranidia and 75 pygidia), and the Procrustes distances from the reference were plotted against the log of the centroid size. The Procrustes distance broadly increases as size increases, but the studied population shows no significant difference between smaller and larger specimens ($p < 0.001$) (Fig. 14a). This confirms the isometric trend seen in the pygidia with RMA and suggests a more isometric trend in the cranidia than the observed allometric trend suggested in RMA (see results and discussion above). The morphologically mature specimens show no significant difference in size range of cranidia or pygidia among species, with the exception of a couple of large specimens from Assemame and several pygidia of *A. levisettii* (Fig. 14b).

6. Discussion

The above-reported morphological analyses (both bivariate and multivariate) demonstrate that *A. mureroensis* can be identified outside its type locality and that the compaction- and tectonic-related deformation does not prevent a confident identification of its precise morphology.

The analysis of the cranidia shows a single and broad morphospecies within the sample (Zamora *et al.*'s (2014) 'mureroensis group'): cranidial features are not considered significant enough to distinguish so many species. However, whereas RMA and PCA analyses of pygidia suggest that *A. pampalius*, *A. levisettii* and *A.* cf. *mureroensis* share the intraspecific variability of *A. mureroensis*, in contrast, the pygidia of *A. nobilis* and *A. ovatopyge* are morphologically distinct from *A. mureroensis*, and its specimens seemingly fall into their own trend. Although RMA of the pygidia shows similar trends in the pattern growths and suggests that there is only one morphospecies, the growth of the pygidial anterior margin seems to have a wider posterior border compared with the rest of the populations. PCA confirms a different trend in the growth of this measurement, suggesting that at least *A. nobilis* (and maybe *A. ovatopyge*) represents a different (but conspecific) taxon. Thus, based on pygidial differences, *A. nobilis* is considered here as a valid taxon. The morphological analysis of the pygidia suggests that *A. pampalius*, *A. levisettii* and *A.* cf. *mureroensis* share the same morphospace and should be considered as junior synonyms of *A. mureroensis*.

Geometric morphometrics provide further specific information about the shape variation of the sample. Such variation is mainly expressed in the shape, orientation and width of the palpebral lobe, the interocular area width (between δ and axial furrow) and the position of the anterior branch of the facial suture (from divergent forms to more convergent forms) relative to the rest of the cranidium. Less important seems to be the glabellar variation. Higher variation is seen in the pygidial sample and mainly concerns the position of the maximum width, which can be more or less in a rear position. The change of the platform position with respect to the posterior border is also important. These features are distinctive, especially the position of the maximum width that the multivariate analysis did not deal with. But it also confirms the variation seen in the pygidial anterior border width (landmarks 1–3). The bootstrapped F-test shows an important difference between *A. nobilis* and the rest of the species; removing this taxon, the position of the maximum width reduces its importance in the general shape of the pygidium, although a variation in the pygidial anterior

border width is still recognized. The position of the maximum width, contrasting with other *Acadoparadoxides* species, is in rear position in *A. nobilis*. On the contrary, *A. ovatopyge* seems to be closer to the rest of *Acadoparadoxides* species, sharing most of its morphospace with the rest of the populations.

The cranidial morphology of *A. mureroensis* from Spain encompasses all the variation expressed by the rest of the species. It is important to emphasize that, in both methods, the holotype falls in the central part of all the morphospace (Figs 6, 7). In addition, *A. levisettii* encompasses most of the variation of the Moroccan species, and the Assemame assemblage overlap throughout all Moroccan species. By contrast, the mean morphology of a few species remains significantly different from others (Table 6). Most of the species do not encompass all the variation of the pygidia, and the Spanish material overlaps most of the morphospace displayed by the Moroccan species, with the exception of *A. nobilis*. The mean morphology of many species is significantly different from others (Table 10). Here we face a classical problem: are these species a single one according to our data? If we had only two species with significantly different means and minimal overlap (e.g. *A. pampalius* and *A. levisettii*), we would state that those samples represent different species diagnosable by a single range of continuous characters (for a previous example of the same problem, see Hopkins & Webster, 2009). Nevertheless, after adding more species and including data by successive pooling of samples, the species cannot be distinguished between them. According to Nixon & Wheeler (1990), most of these species should not be distinct from each other: e.g. *A. nobilis* is significantly different from all *Acadoparadoxides* species, even after bootstrapping. These results do not allow recognition of the newer species: any specimen falling within areas of overlap could not be diagnosed as a member of any particular species. In the Assemame open quarry, all the morphotypes diagnosed as different species, but overlapped morphologically, are found within the same stratigraphic level. Thus, these analyses point to the distinction of only two species (*A. mureroensis* and *A. nobilis*) exhibiting some gradual morphological variations in the pygidia, the former including previous species designated to *A. cf. mureroensis*, *A. levisettii*, *A. ovatopyge* and *A. pampalius.*

In addition, the semi-landmark analysis shows a remarkable resemblance between the mean shapes of the pygidia (Table 12). Once more, the mean shape of *A. nobilis* is distinct and differentiable, and statistically representative (see Goodall's test), from the rest of the analysed species. The mean pygidial shape of *A. levisettii* is somewhat statistically differentiable, whereas with the above-reported morphometric analysis it was only significantly different from the Assemame assemblage. This may be a consequence of size bias because the specimens of *A. levisettii* are represented by a wider range of sizes (Fig. 14). Therefore, allometry may explain most of the variation shown by

all the populations with the exception of *A. levisettii* (Table 11).

In summary, based on the revised diagnostic characters and the 2D biometrical assessment discussed above, *A. ovatopyge*, *A. pampalius* and *A. cf. mureroensis* should be considered as junior species of *A. mureroensis*, and *A. nobilis* as a valid species. Both species overlap stratigraphically neither in the Tarhoucht nor Assemame quarries (for the former quarry, see stratigraphic ranges in Geyer & Vincent, 2014, fig. 8). *Acadoparadoxides nobilis* has not yet been reported in the Iberian Chains. Larger specimens of *A. ovatopyge*, *A. pampalius* and *A. mureroensis* are necessary to complete an accurate comparison with *A. levisettii*, though, based on the overlapping morphospace displayed by this species in the above-reported analyses, we also suggest this species might be a synonym of *A. mureroensis.*

7. Systematic palaeontology

The morphological terms used below follow Whittington *et al.* (1997) and are illustrated in Figure 4. Illustrated and reported material from Assemame is housed in the IGME Museum, Río Rosas 23, Madrid (acronyms MGM).

Family Paradoxididae Hawle & Corda, 1847
Subfamily Paradoxidinae Hawle & Corda, 1847
Genus *Acadoparadoxides* Šnajdr, 1957

Type species. *Paradoxides sacheri* Barrande, 1852 from the middle Cambrian Jince Formation, Czech Republic (by original designation).

Discussion. The diagnoses of paradoxidinine genera are still a matter of discussion due to the allometric trends displayed during the ontogeny and the morphological variation exhibited by some of their species, which make difficult their subdivision based on the relative proportions of cranidia and pygidia. Consequently, some diagnostic characters of one adult species can occur during different ontogenetic stages in another species (e.g. see recent synonymy of two species sharing diagnostic characters of *Acadoparadoxides* and *Eccaparadoxides* by Esteve, 2014). Šnajdr's (1957, 1958, 1986, 1987), Sdzuy's (1967) and Solov'ev's (1980) concept of *Acadoparadoxides* includes: (1) S1 and S2 glabellar furrows medially (or nearly) connected, (2) palpebral lobes reaching the posterior border furrow, (3) distance between the anterolateral corners of the cranidium with similar width to the greatest width across palpebral lobes, (4) poorly segmented pygidial axis, and (5) a pygidial axis at least 50 % of the pygidial length (for a historical revision of the genus, see Geyer & Vincent, 2014). Provisionally, we follow the above-reported five points.

Acadoparadoxides mureroensis (Sdzuy, 1958)
Figures 15, 16a–k, 17a–n

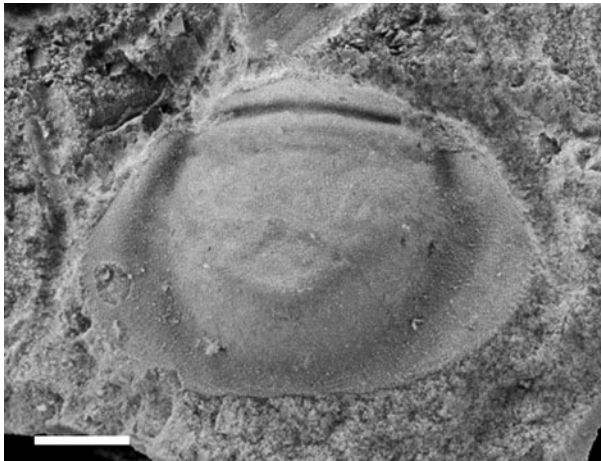New material. Fifteen cranidia, seven pygidia attached to incomplete thoraxes and eight disarticulated pygidia

Figure 15. Internal mould in dorsal view of *Acadoparadoxides mureroensis* selected topotype (pygidium) from the type section in Murero (MPZ2004/59); scale = 2 mm.

preserved as internal and external moulds in marly shales.

Holotype. Sdzuy (1958), pl. 1, fig. 12, cranidium from the Valdemiedes section in Murero, Iberian Chains, NE Spain.

Paratype. Sdzuy (1958), pl. 1, fig. 13, pygidial syntype from the Valdemiedes section in Murero, Iberian Chains, NE Spain (Fig. 14).

Emended diagnosis (in 2D). Species of *Acadoparadoxides* with width of anterior lobe *c.* 70 % of glabellar length; posterior glabellar width moderately narrow, *c.* 50 % of glabellar length; posterior branch of facial suture very short, *c.* 8 % of glabellar length; ocular lobe *c.* 40 % (sag.) of glabellar length. Thorax with up to 19 segments; pleurae with short horizontal inner portion, fulcra absent in posterior segments; short pleural furrow extending abaxially to edge of doublure piercing slightly doublure of anterior segments; large pleural spines increasing in length anteriorly, from *c.* 60 % of segment width (tr.) to *c.* 80 % in posterior part; posteriormost pleural spines flank pygidium and reach beyond level of pygidial edge. Pygidium with variable outline, grading from subtriangular to
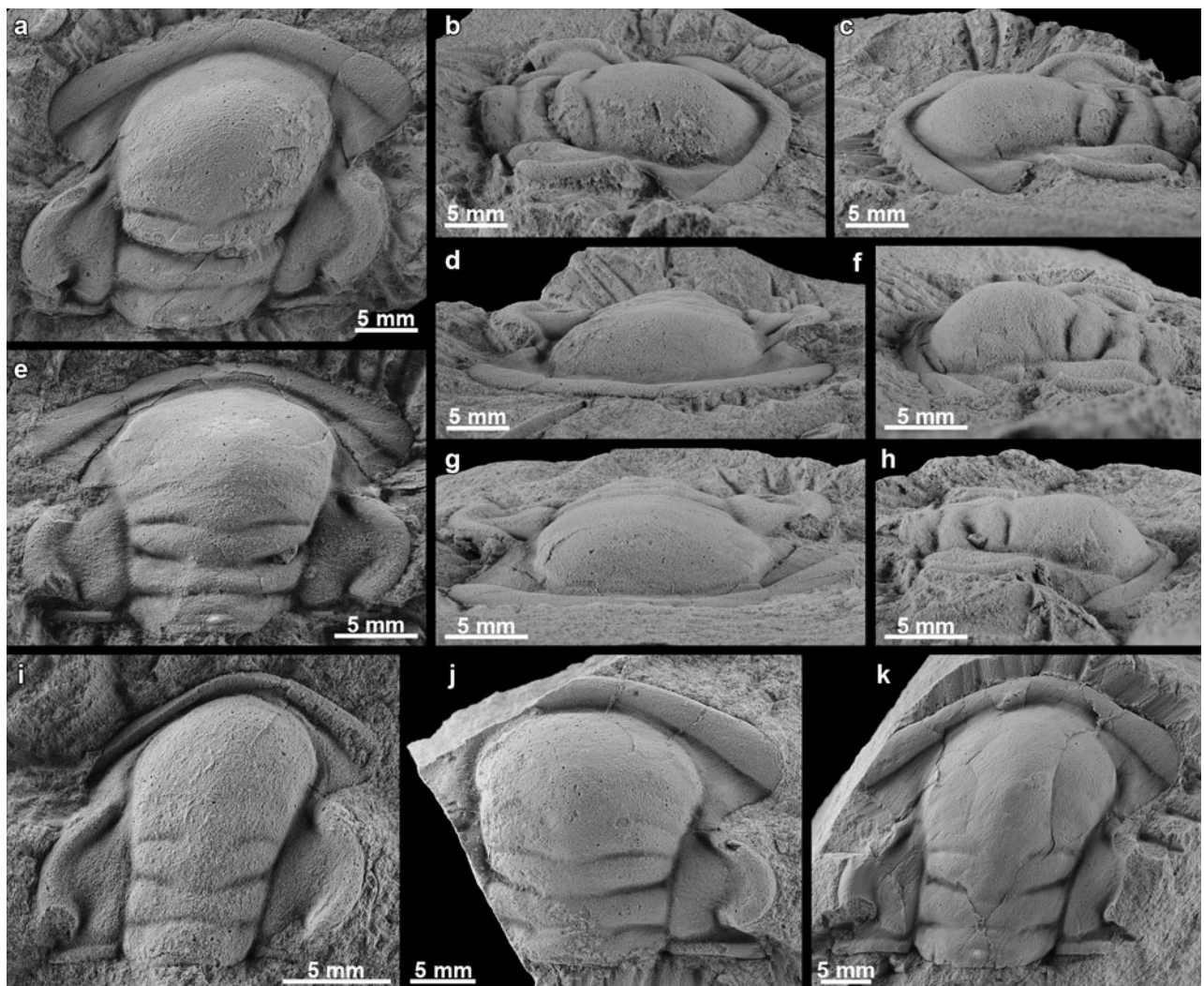

Figure 16. Cranidia of *Acadoparadoxides mureroensis* (Sdzuy, 1958) from the Assemame quarry; internal moulds. (a–d) MGM-6794X (a – dorsal view, b – right lateral view, c – left lateral view, d – frontal view), (e–h) MGM-6795X (e – dorsal view, f – left lateral view, g – frontal view, h – right lateral view), (i) MGM-6796X, dorsal view; (j) MGM-6797X, dorsal view; (k) MGM-6798X, dorsal view.
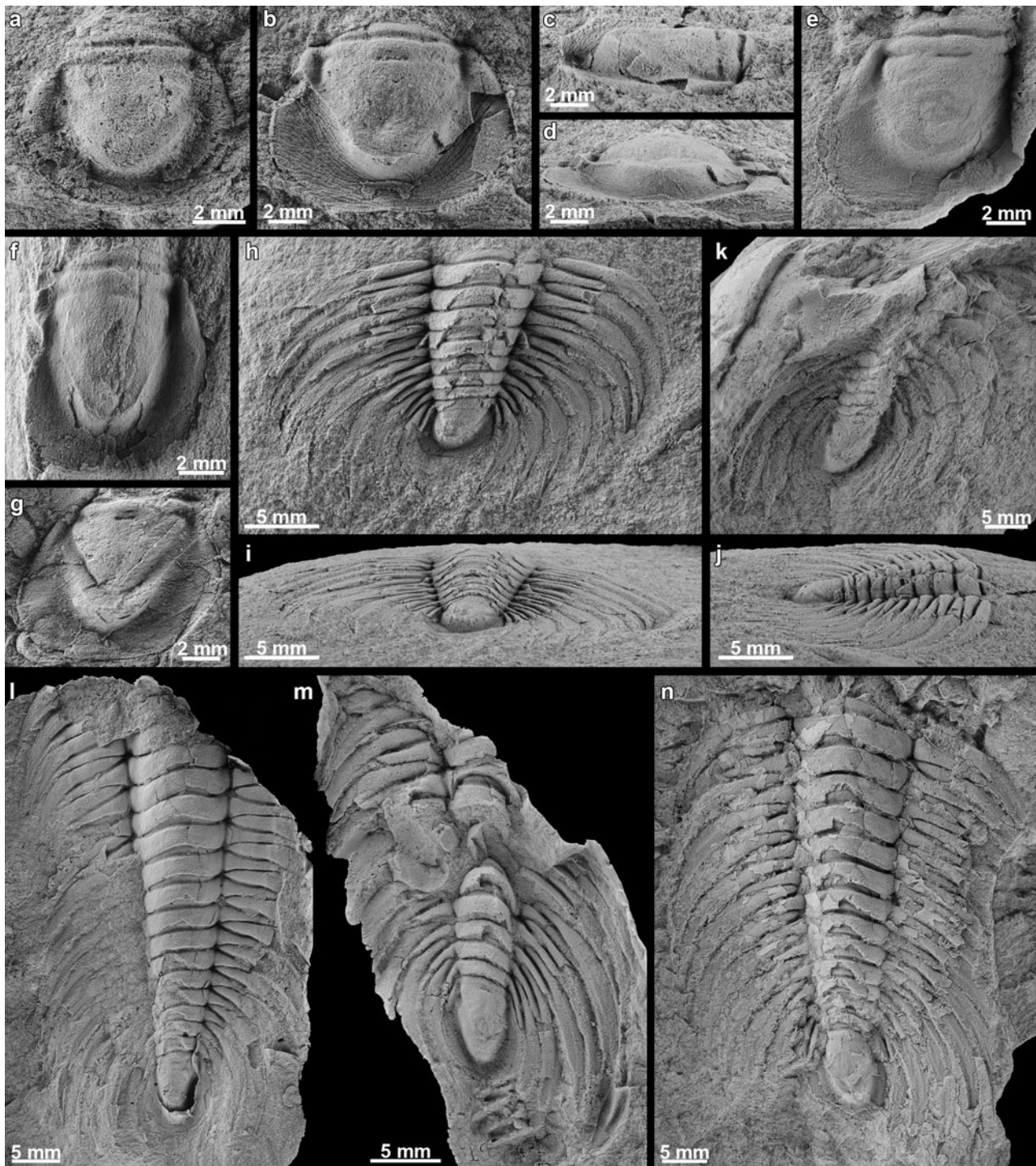
Figure 17. Pygidia of *Acadoparadoxides mureroensis* (Sdzuy, 1958) from the Assemame quarry. (a) MGM-6799X, dorsal view of internal mould; (b–d) MGM-6800X, internal mould (b - dorsal view, c - lateral view, d - posterior view); (e) MGM-6801X, dorsal view of latext cast; (f) MGM-6802X, dorsal view of internal mould; (g) MGM-6803X, internal mould; (h–j) MGM-6804X, internal mould of an articulated pygidium with posterior thoracic segments (h - dorsal view, i - posterior view, j - lateral view); (k) MGM-6805X, dorsal view of internal mould; (l–n) MGM-6806X to 6808X, internal moulds of an articulated pygidium with posterior thoracic segments.

subhexagonal and subovate; posterior margin with straight section to slightly rounded; rachis subtriangular in outline, 55–80 % of pygidial length, with one axial ring recognizable, and occasionally with a second poorly developed axial ring.

Description. Exoskeleton broadly to elongately oval in outline, evenly rounded anteriorly; largest size (sag.) up to 30 cm. Cephalon semicircular, moderately short, *c.* 30–45 % (decreasing with growth) of total length. Cranidium as wide as long or slightly wider; anterior

margin evenly curved to subarcuate and posterior margin nearly straight (tr.). Glabella clavate in shape, rounded anteriorly; *c.* 90 % of cranidial length (including occipital ring) and 40 % of cranidial width across centre of palpebral lobes; glabellar frontal lobe *c.* 1.25–1.45 times width of occipital ring; four glabellar furrows, well marked, with transglabellar S1 and S2, and S3 and S4 not transglabellar, sometimes barely visible; occipital ring short, *c.* 15 % (sag.) of cephalic length, with some specimens bearing small occipital node; occipital furrow shallow. Anterior border narrow, *c.* 10 % (sag.) of glabellar length, slightly convex, with narrow anterior border furrow. Preglabellar field very short in late meraspids, *c.* 5 % of glabellar length, disappearing in holaspids. Palpebral area moderately wide, *c.* 15–30 % (decreasing with growth) of posterior cranidial width; eye lobes *c.* 35–45 % of cranidial length; lack of postocular area and very narrow preocular area, with posterolateral projection very short, *c.* 5 % of cephalic length and 10 % of glabellar width. Palpebral lobe crescentic in outline and moderately long, *c.* 40 % of glabellar length. Anterior branch of facial suture divergent from palpebral lobes at angle of *c.* 45° to sagittal line; posterior branch divergent at angle of *c.* 110° to sagittal line.

Thorax with up to 19 segments; pleural furrow well-defined and deep; anterior and posterior pleural bands well-marked; pleural segments slightly curving progressively backward; posteriormost two to three segments narrowing and curved more strongly backward. Pleural segments gently curved backward, with very long pointed pleural spine.

Pygidium grading from sub-rounded to sub-hexagonal and subovate in outline, with posterior margin slightly rounded to straight; posterior border flat or evenly curved; base of pygidial pleurae and posteroaxial area broadly flat to slightly depressed; rachis subtriangular in outline, moderately long but highly variable, *c.* 55–80 % of pygidial length with one axial ring recognizable; occasionally with one or two poorly developed axial rings; terminal piece sub-rounded to subacute in outline.

Comparison. *A. mureroensis* differs from *A. nobilis* in its flat and slightly rounded to straight posterior margin of pygidium (which contrasts with the slight median indentation displayed by the latter species), and the position of the horizontal line linking the widest (tr.) points of the pygidium (more posterior in *A. nobilis* so proportionately longer to the sagittal length).

Despite the absence of 3D morphometrics analysis in this work, necessary to quantify two diagnostic characters of the cranidial and pygidial reliefs stated by Geyer & Vincent (2014) (the relative convexity of the cranidial anterior border and the concave base of the pygidial pleurae and posteroaxial area forming a slight bowl-shaped depression in the pygidium), these 3D characters are not reliable when comparing material preserved in shales (see Geyer & Vincent, 2014, fig. 22e, g) and should be statistically checked in order to distinguish *A. pampalius* and *A. levissettii* from *A.*

mureroensis. Unfortunately, the preservation in shales of our flattened study material prevents any confident 3D analysis, which should be done in material preserved in silica nodules and/or carbonates.

8. Conclusions

A statistical revision based on bivariate (RMA) and principal component (PCA) analyses and geometric morphometrics (LM and SLM) was performed on the earliest paradoxinine trilobites that mark the diachronous immigration of 'mid Cambrian' trilobites in the western Mediterranean region. The latter marks the base of the regional middle Cambrian in Spain and, based on Hupé's (1960) chronostratigraphic chart, in Morocco. The morphological analysis has taken into account the different degree of deformation of the Iberian and Moroccan trilobites, which does not preclude a taxonomic comparison of the Iberian and Moroccan species. As a result, the diagnosis of *A. mureroensis* is emended and a synonymy with *A.* cf. *mureroensis*, *A. levisettii*, *A. ovatopyge* and *A. pampalius* is suggested based on 2D morphological characters. The FAD of *A. mureroensis* in both areas can be provisionally used for regional correlation until homotaxic tests to check its possible diachronism are done.

References

ABRÀMOFF, M. D., MAGALHÃES, P. J. & RAM, S. J. 2004. Image processing with ImageJ. *Biophotonics International* **11**(7), 36–42.

ÁLVARO, J. J. 2007. New ellipsocephalid trilobites from the lower Cambrian member of the Láncara Formation, Cantabrian Mountains, northern Spain. *Memoirs of the Association of Australasian Palaeontologists* **34**, 29–41.

ÁLVARO, J J. 2014. Rift, pull-apart rift, and continental drift crossword puzzles across the lower–middle Cambrian transition of Iberia and Morocco. *GFF* **136**(1), 2–5.

ÁLVARO, J. J., BENZIANE, F., THOMAS, A. R., WALSH, G. J. & YAZIDI, A. 2014. Neoproterozoic–Cambrian stratigraphic framework of the Anti-Atlas and Ouzellagh promontory (High Atlas), Morocco. *Journal of African Earth Sciences* **98**, 19–33.

ÁLVARO, J. J. & CLAUSEN, S. 2005. Major geodynamic and sedimentary constraints on the chronostratigraphic correlation of the Lower–Middle Cambrian transition in the

western Mediterranean region. *Geosciences Journal* **9**, 145–60.

ÁLVARO, J. J. & CLAUSEN, S. 2006. Microbial crusts as indicators of stratigraphic diastems in the Cambrian Micmacca Breccia, Moroccan Atlas. *Sedimentary Geology* **185**, 255–65.

ÁLVARO, J. J. & CLAUSEN, S. 2008. Paleoenvironmental significance of Cambrian hiatal shell accumulations in an aborted intra-cratonic rift, Atlas Mountains, Morocco. In *Dynamics of Epeiric Seas* (ed. B. R. Pratt & C. Holmden), pp. 39–54. Geological Association of Canada, Special Paper no. 48.

ÁLVARO, J. J., ELICKI, O., GEYER, G., RUSHTON, A. W. A. & SHERGOLD, J. H. 2003. Palaeogeographical controls on the Cambrian trilobite immigration and evolutionary patterns reported in the western Gondwana margin. *Palaeogeography, Palaeoclimatology, Palaeoecology* **195**, 5–35.

ÁLVARO, J. J., EZZOUHAIRI, H., CLAUSEN, S., RIBEIRO, M. L. & SOLÁ, R. 2015. Syn-rift unconformities punctuating the lower–middle Cambrian transition of the Atlas Rift, Morocco. *International Journal of Earth Sciences* **104**(3), 752–73.

ÁLVARO, J. J., GOZALO, R., LIÑÁN, E. & SDZUY, K. 1993. The palaeogeography of northern Iberia at the Lower–Middle Cambrian transition. *Bulletin de la Société Géologique de France* **164**, 843–50.

ÁLVARO, J. J. & VENNIN, E. 1996. Tectonic control on Cambrian sedimentation in south-western Europe. *Eclogae Geologica Helvetiae* **89**, 935–48.

ÁLVARO, J. J. & VENNIN, E. 1997. Episodic development of Cambrian eocrinoid-sponge meadows in the Iberian Chains (NE Spain). *Facies* **37**, 49–64.

ÁLVARO, J. J., VENNIN, E., MUÑOZ, A., SÁNCHEZ-VALVERDE, B. & OJEDA, J. L. 2000. Interplay of orbital forcing and tectonic pulses in the Cambrian Iberian platform, NE Spain. *International Journal of Earth Sciences* **89**, 366–76.

BARRANDE, J. 1852. *Système Silurien du centre de la Bohême. Ière partie*. Prague and Paris: Recherches Paléontologiques, 935 pp.

BERGSTRÖM, J. & LEVI-SETTI, R. 1978. Phenotypic variation in the Middle Cambrian trilobite *Paradoxides davidis* Salter at Manuels, SE Newfoundland. *Geologica et Palaeontologica* **12**, 1–40.

BONDON, J. & NELTNER, L. 1933. Sur la série cambrienne des plateaux de Drâa (Sud Marocain) et la présence du Géorgien dans cette série. *Comptes Rendus de l'Académie des Sciences, Paris* **197**, 170–2.

BOOKSTEIN, F. L. 1991. *Morphometric Tools for Landmark Data*. New York: Cambridge University Press.

BRIGGS, D. E. G. & WILLIAMS, S. H. 1981. The restoration of flattened fossils. *Lethaia* **14**, 157–64.

BRØGGER, W. C. 1879. Om Paradoxidesskifrene ved Krekling. *Nyt Magazin Naturvidenskap* **24**, 18–88.

BRØGGER, W. C. 1886. Om alderen af Olelluszonen i Nordamerika. *Geologiska Föreningens i Stockholm Förhandlingar* **8**, 182–213.

BUGGISCH, W., MARZELA, C. & HÜGEL, P. 1978. Die fazielle und paläogeographische Entiwocklung der infrakambrischen bis ordovizischen Sedimente im Mittleren Antiatlas um Agdz (S-Marokko). *Geologische Rundschau* **68**, 195–224.

CHOUBERT, G. 1963. *Histoire géologique du Précambrien de l'Anti-Atlas*. Notes et Mémoires du Service Géologique du Maroc no. 162, 352 pp.

CLAUSEN, S. & ÁLVARO, J. J. 2002. Encrusting strategies in a Cambrian nonreefal epibenthic community. *Bulletin de la Société Géologique de France* **173**, 553–9.

CLAUSEN, S., ÁLVARO, J. J. & ZAMORA, S. 2014. Replacement of benthic communities in two Neoproterozoic–Cambrian subtropical-to-temperate rift basins, High Atlas and Anti-Atlas, Morocco. *Journal of African Earth Sciences* **98**, 72–93.

CLAUSEN, S. & SMITH, A. B. 2008- Stem structure and biological affinities of a Cambrian problematic deuterostome (Stylophora). *Nature* **438**, 351–4.

COOPER, R. A. 1970. Tectonic distortion of a syntype of *Isograptus forcipiformis latus* Ruedemann. *Journal of Paleontology* **44**, 980–3.

COOPER, R. A. 1990. Interpretation of tectonically deformed fossils. *New Zealand Journal of Geology and Geophysics* **33**, 321–32.

DEAN, W. T. & ÖZGUL, N. 1994. Cambrian rocks and faunas, Hüdai area, Taurus Mountains, southwestern Turkey. *Bulletin de l'Institut Royal des Sciences Naturelles de Belgique, Sciences de la Terre* **64**, 5–20.

DESTOMBES, J., HOLLARD, H. & WILLEFERT, S. 1985. Lower Palaeozoic rocks of Morocco. In *Lower Palaeozoic Rocks of the World, vol. 4: Lower Palaeozoic of North-Western and West Central Africa* (ed. C. H. Holland), pp. 57–184. Chichester: John Wiley and Sons.

DRYDEN, I. L. & MARDIA, K. V. 1998. *Statistical Shape Analysis*. New York: John Wiley & Sons, 347 pp.

ESTEVE, J. 2014. Intraspecific variability in paradoxidid trilobites from the Purujosa trilobite assemblage (middle Cambrian, northeast Spain). *Acta Palaeontologica Polonica* **59**, 215–40.

FOOTE, M. 1991. Morphological patterns of diversification – examples from trilobites. *Palaeontology* **34**, 461–8.

GEYER, G. 1988. Agnostida aus dem höheren Unterkambrium und dem Mittelkambrium von Marokko. Teil 2: Eodiscina. *Neues Jahrbuch für Geologie und Paläontologie, Abhandlungen* **177**, 93–133.

GEYER, G. 1989. Late Precambrian to early Middle Cambrian lithostratigraphy of southern Morocco. *Beringeria* **1**, 115–43.

GEYER, G. 1990. Revised Lower to lower Middle Cambrian biostratigraphy of Morocco. *Newsletters on Stratigraphy* **22**, 53–70.

GEYER, G. 1993. The giant Cambrian trilobites of Morocco. *Beringeria* **8**, 71–107.

GEYER, G. 1998. Intercontinental, trilobite-based correlation of the Moroccan early Middle Cambrian. *Canadian Journal of Earth Sciences* **35**, 374–401.

GEYER, G. 2006. First African oryctocephalid trilobites from the Lower–Middle Cambrian boundary interval. *Palaeoworld* **15**, 348–59.

GEYER, G. & LANDING, E. (eds) 1995. *Morocco'95. The Lower–Middle Cambrian Standard of Gondwana*. Beringeria, Special Issue 2, 171 pp.

GEYER, G. & LANDING, E. 2001. Middle Cambrian of Avalonian Massachusetts: stratigraphy and correlation of the Braintree trilobites. *Journal of Paleontology* **75**, 116–35.

GEYER, G. & LANDING, E. 2004. A unified Lower–Middle Cambrian chronostratigraphy for West Gondwana. *Acta Geologica Polonica* **54**, 179–218.

GEYER, G. & LANDING, E. (eds) 2006. *Ediacaran–Cambrian depositional environments and stratigraphy of the western Atlas regions*. Beringeria, Special Issue 6, 120 pp.

GEYER, G. & VINCENT, T. 2014. The *Paradoxides* puzzle resolved: the appearance of the oldest paradoxidines and

its bearing on the Cambrian Series 3 lower boundary. *Paläontologische Zeitschrift* **89**(3), 335–98.

GOODALL, C. 1991. Procrustes methods in the statistical analysis of shape. *Journal of the Royal Statistical Society, Series B: Methodological* **53**, 285–339.

GOZALO, R., DIES ÁLVAREZ, M. E., GÁMEZ VINTANED, J. A., ZHURAVLEV, A. YU., BAULUZ, B., SUBÍAS, I., CHIRIVELLA MARTORELL, J. B., MAYORAL, E., GURSKY, H. J., ANDRÉS, J. A. & LIÑÁN, E. 2013. Proposal of a reference section and point for the Cambrian Series 2–3 boundary in the Mediterranean subprovince in Murero (NE Spain) and its intercontinental correlation. *Geological Journal* **48**, 142–55.

GOZALO, R., LIÑÁN, E. & DÍES, M. E. 2003. Intraspecific dimorphism and evolutionary series of paradoxidids from the Middle Cambrian of Murero, Spain. *Special Papers in Palaeontology* **70**, 141–56.

GOZALO, R., LIÑÁN, E., DIES ÁLVAREZ, M. E., GÁMEZ VINTANED, J. A. & MAYORAL, E. 2007. The Lower–Middle Cambrian boundary in the Mediterranean subprovince. In *The Evolution of the Rheic Ocean: From Avalonian–Cadomian Active Margin to Alleghenian–Variscan Collision* (ed. U. Linnemann, R. D. Nance, P. Kraft & G. Zulauf), pp. 359–73. Geological Society of America, Special Paper no. 423.

HAMMER, Ø. & HARPER, D. A. T. 2006. *Paleontological Data Analysis*. Oxford: Blackwell.

HAWLE, I. & CORDA, A. J. C. 1847. Prodom einer Monographie der böhmischen Trilobiten. *Abhandlungen der Königlichen Nöhmischen Gesselschaft der Wissenschaften* **5**, 1–176.

HOPKINS, M. J. & WEBSTER, M. 2009. Ontogeny and geographic variation of a new species of the corynexochine trilobite *Zacanthopsis* (Dyeran, Cambrian). *Journal of Paleontology* **83**(4), 524–47.

HUGHES, N. C. 1991. Morphological plasticity and genetic flexibility in a Cambrian trilobite. *Geology* **19**, 913–16.

HUGHES, N. C. 1994. Ontogeny, intraspecific variation, and systematics of the Late Cambrian trilobite *Dikelocephalus*. *Smithsonian Contributions to Paleobiology* **79**, 1–89.

HUGHES, N. C. & JELL, P. A. 1992. A statistical/computer-graphic technique for assessing variation in tectonically deformed fossils and its application to Cambrian trilobites from Kashmir. *Lethaia* **25**, 317–30.

HUGHES, N. C. & JELL, P. A. 1999. The biostratigraphy and biogeography of Himalayan Cambrian trilobites. In *Himalaya and Tibet: Mountain Roots to Mountain Tops* (ed. A. Macfarlane, R. B. Sorkhabi & J. Quade), pp. 109–16. Geological Society of America, Special Paper no. 328.

HUGHES, N. C. & RUSHTON, A. W. A. 1990. Computer-aided restoration of a Late Cambrian ceratopygid trilobite from Wales, and its phylogenetic implications. *Palaeontology* **33**, 429–45.

HUPÉ, P. 1953. *Contribution à l'étude du Cambrien inférieur et du Précambrien III de l'Anti-Atlas marocain*. Notes et Mémoires du Service Géologique du Maroc no. 103, 402 pp.

HUPÉ, P. 1960. Sur le Cambrien inférieur du Maroc. *Reports of the 21st Session of the International Geological Congress, Part VIII (Proceedings of Section 8), Copenhagen*, 75–85.

JEFFERIES, R. P. S., LEWIS, M. & DONOVAN, S. K. 1987. *Protocystites menevensis* – a stem-group chordate (Cornuta) from the Middle Cambrian of South Wales. *Palaeontology* **30**, 429–84.

JELL, P. A. & HUGHES, N. C. 1997. Himalayan Cambrian trilobites. *Special Papers in Palaeontology* **58**, 1–113.

KIM, K., SHEETS, D. H. & MITCHELL, C. E. 2009. Geographic and stratigraphic change in the morphology of *Triarthus beckii* (Creen) (Trilobita): a test of *Plus ça change* model of evolution. *Lethaia* **42**, 108–25.

LABANDEIRA, C. C. & HUGHES, N. C. 1994. Biometry of the Late Cambrian trilobite genus *Dikelocephalus* and its implications for trilobite systematics. *Journal of Paleontology* **68**, 492–517.

LIÑÁN, E. & GOZALO, R. 1986. Trilobites del Cámbrico Inferior y Medio de Murero (Cordillera Ibérica). *Memorias del Museo Paleontológico de la Universidad de Zaragoza* **2**, 1–104.

LIÑÁN, E., PEREJÓN, A. & SDZUY, K. 1993. The Lower–Middle Cambrian stages and stratotypes from the Iberian Peninsula: a revision. *Geological Magazine* **130**, 817–33.

LOTZE, F. 1961. Das Kambrium Spaniens. Teil I: Stratigraphie. *Akademie der Wissenschaften und der Literatur Abhandlungen der Mathematisch-Natursissenschaftilichen Klasse* (for 1961) **6**, 381–498.

MARDIA, K. V., KENT, T. J. & BIBBLY, J. M. 1994. *Multivariate Analysis*. London: Academic Press.

NIXON, K. & WHEELER, Q. D. 1990. An amplification of the phylogenetic species concept. *Cladistics* **6**, 211–23.

ÖZDIKMEN, H. 2009. Nomenclatural changes for twenty trilobite genera. *Munis Entomology & Zoology* **4**, 155–71.

PALMER, A. R. 1957. Ontogenic development of two olenellid trilobites. *Journal of Paleontology* **31**, 105–28.

PENG, S. C., BABCOCK, L. E., ZHU, X. J., AHLBERG, P., TERFELT, F. & DAI, T. 2015. Intraspecific variation and taphonomic alteration in the Cambrian (Furongian) agnostoid *Lotagnostus americanus*: new information from China. *Bulletin of Geosciences* **90**, 281–306.

RASETTI, F. 1948. Lower Cambrian trilobites from the conglomerates of Quebec (exclusive of the Ptychopariidae). *Journal of Paleontology* **22**, 1–24.

ROHLF, F. J. 1990. Rotational fit (Procrustes) methods. In *Proceedings of the Michigan Morphometrics Workshop* (ed. F. J. Rohlf & F. L. Bookstein), pp. 227–36. University of Michigan Museum of Zoology, Special Publication no. 2.

SDZUY, K. 1958. Neue trilobiten aux dem Mittelkambrium von Spanien. *Senckenbergiana lethaea* **39**, 235–53.

SDZUY, K. 1961. Das Kambrium Spaniens. Teil II: Trilobiten. *Akademie der Wissenschaften und der Literatur Abhandlungen der Mathematisch-Natursissenschaftilichen Klasse* (for 1961) **7**, 217–312.

SDZUY, K. 1966. An improved method of analysing distortion in fossils. *Palaeontology* **9**, 125–34.

SDZUY, K. 1967. Trilobites del Cámbrico medio de Asturias. *Trabajos de Geología, Universidad de Oviedo* **1**, 77–133.

SDZUY, K. 1971a. Acerca de la correlación del Cámbrico inferior en la Península Ibérica. *I Congreso Hispano-Luso-Americano de Geología Económica, Geología* **2**, 753–66.

SDZUY, K. 1971b. La subdivisión bioestratigráfica y la correlación del Cámbrico medio en España. *I Congreso Hispano-Luso-Americano de Geología Económica, Geología* **2**, 769–82.

SDZUY, K. 1972. Das Kambrium der Acadobaltischen Faunenprovinz. *Zentralblatt für Geologie und Paläontologie* **2**, 1–91.

SHEETS, H. D. 2014. *Integrated Morphometrics Package*. Buffalo, NY: Canisius College.

SMITH, A. B., ZAMORA, S. & ÁLVARO, J. J. 2013. The oldest echinoderm faunas from Gondwana show echinoderm body plan diversification was rapid. *Nature Communications* **4**, 1385. doi: 10.1038/ncomms2391.

ŠNAJDR, M. 1957. O nových trilobitech z českého kambria. *Věstník Ústředního Ústavu Geologického* **32**, 235–44.

ŠNAJDR, M. 1958. Trilobiti českého středního kambria. *Rozpravy Ústředního Ústavu Geologického* **24**, 1–174.

ŠNAJDR, M. 1986. Two new paradoxidid trilobites from the Jince Formation (Middle Cambrian, Czechoslovakia). *Věstník Ústředního Ústavu Geologického* **61**, 169–74.

ŠNAJDR, M. 1987. The genera *Paradoxides* Brogniart and *Hydrocephalus* Barrande (Trilobita). *Věstník Ústředního Ústavu Geologického* **62**, 97–104.

SOLOV'EV, I. A. 1980. *Trilobity semeystva Paradoxididae i ikh znachenie dlya stratigrafii kembriyskikh otlozheniy*. Leningrad, Avtoreferat dissertatsiina soiskanie uchenoi stepeni kandidata geologo-mineralicheskikh nauk, 22 pp. Published thesis (in Russian).

SRIVASTAVA, D. C. & SHAH, J. 2006. Digital method for strain estimation and retrodeformation of bilaterally symmetric fossils. *Geology* **34**, 593–6.

WEBSTER, M. 2007. A Cambrian peak in morphological variation within trilobite species. *Science* **317**(5837), 499–502.

WEBSTER, M. & HUGHES, N. C. 1999. Compaction-related deformation in Cambrian olenelloid trilobites and its implications for fossil morphometry. *Journal of Paleontology* **73**, 355–71.

WEBSTER, M. & SHEETS, H. D. 2010. A practical introduction to landmark-based geometric morphometrics. In *Quantitative Methods in Paleobiology* (ed. J. Alroy & G. Hunt), pp. 163–88. *The Paleontological Society Papers* **16**.

WEIDNER, T. & NIELSEN, A. T. 2009. The Middle Cambrian *Paradoxides paradoxissimus* Superzone on Oland, Sweden. *GFF* **131**, 253–68.

WEIDNER, T. & NIELSEN, A. T. 2014. A highly diverse trilobite fauna with Avalonian affinities from the Middle Cambrian Acidusus atavus Zone (Drumian Stage) of Bornholm, Denmark. *Journal of Systematic Palaeontology* **12**, 23–92.

WHITTINGTON, H. B., CHATTERTON, B. D. E., SPEYER, S. E., FORTEY, R. A., OWENS, R. M., CHANG, W. T., DEAN, T., JELL, P. A., LAURIE, J. R., PALMER, A. R., REPINA, L. N., RUSHTON, A. W. A., SHERGOLD, J. H., CLARKSON, E. N. K., WILMOT, N. V. & KELLY, S. R. A. 1997. *Trilobita. Introduction, Order Agnostida, Order Redlichiida. Treatise on Invertebrate Paleontology, Part O, Revised, vol. 1*. Lawrence, KS: University of Kansas; New York: Geological Society of America, xxiv+530 pp.

ZAMORA, S., ÁLVARO, J. J., CLAUSEN, S. & ESTEVE, J. 2014. Open quarry of the Brèche à Micmacca Member crossing the 'telesto level' at Assemame, central Anti-Atlas. In *Stratigraphic Overview of the Ediacaran and Cambrian from the Anti-Atlas, Morocco* (ed. L. Devaere, S. Clausen & J. J. Álvaro), pp. 72–5. Lille: University of Lille I.

ZELDITCH, M., SWIDERSKI, D., SHEETS, D. H. & FINK, W. 2012. *Geometric Morphometrics for Biologists*. San Diego, CA: Academic Press.